

*An assessment of the Brazil Current  
baroclinic structure and variability near  
22° S in Distinct Ocean Forecasting and  
Analysis Systems*

**Mateus O. Lima, Mauro Cirano,  
Mauricio M. Mata, Marlos Goes,  
Gustavo Goni & Molly Baringer**

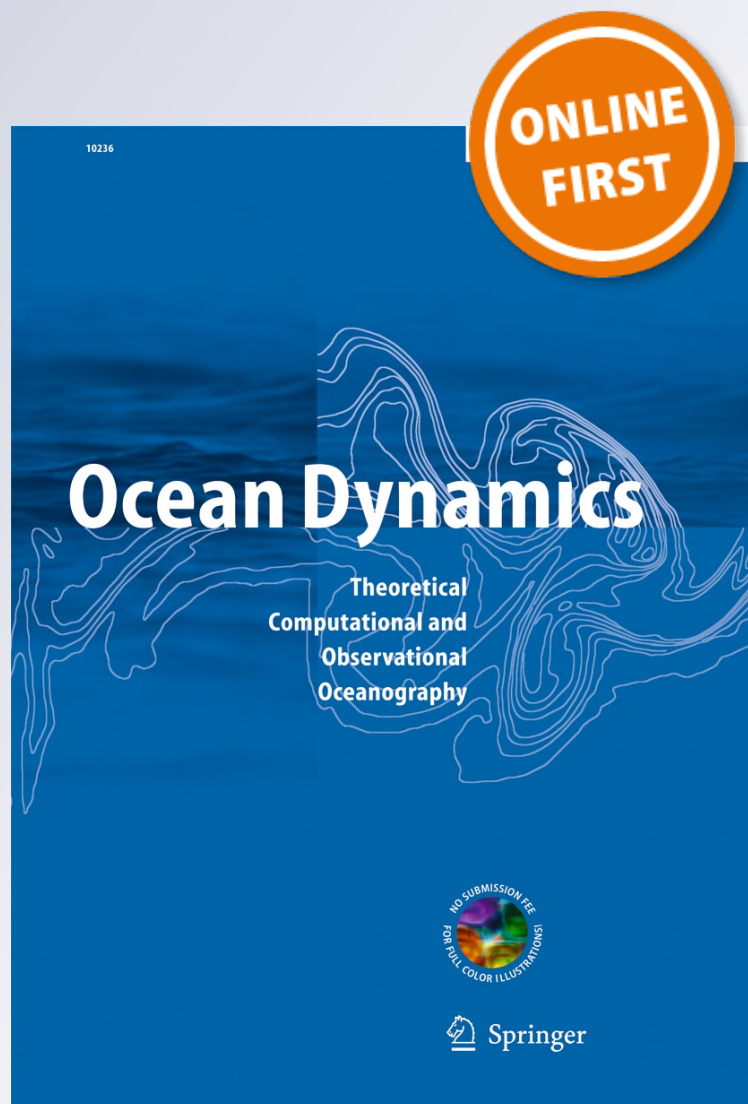
**Ocean Dynamics**

Theoretical, Computational and  
Observational Oceanography

ISSN 1616-7341

Ocean Dynamics

DOI 10.1007/s10236-016-0959-6



**Your article is protected by copyright and all rights are held exclusively by Springer-Verlag Berlin Heidelberg. This e-offprint is for personal use only and shall not be self-archived in electronic repositories. If you wish to self-archive your article, please use the accepted manuscript version for posting on your own website. You may further deposit the accepted manuscript version in any repository, provided it is only made publicly available 12 months after official publication or later and provided acknowledgement is given to the original source of publication and a link is inserted to the published article on Springer's website. The link must be accompanied by the following text: "The final publication is available at [link.springer.com](http://link.springer.com)".**

# An assessment of the Brazil Current baroclinic structure and variability near 22° S in Distinct Ocean Forecasting and Analysis Systems

Mateus O. Lima<sup>1,2</sup> · Mauro Cirano<sup>1,2,3</sup> · Mauricio M. Mata<sup>4</sup> · Marlos Goes<sup>5,6</sup> · Gustavo Goni<sup>5</sup> · Molly Baringer<sup>5</sup>

Received: 30 June 2015 / Accepted: 7 May 2016  
© Springer-Verlag Berlin Heidelberg 2016

**Abstract** The Brazil Current (BC) is the Western Boundary Current of the South Atlantic subtropical gyre, the dominant dynamic feature in the South Atlantic Ocean. The importance of this current lies in that it is the main conduit of subtropical waters to higher latitudes in the South Atlantic Ocean. This study assesses the structure and variability of the BC across the nominal latitude of 22° S using data from the high-density expendable BathyThermograph (XBT) AX97 transect and from three numerical ocean models with data assimilation. This XBT transect was implemented in 2004 and represents one of the longer-term monitoring systems of the BC in existence. The goal of this work is to enhance the understanding of the temporal and spatial variability of the ocean dynamics in the southwestern

South Atlantic Ocean by using a suite of hydrographic observations and numerical model outputs. In the present work, 37 XBT transect realizations using data collected between 2004 and 2012 are used. Daily outputs covering the same time period are evaluated from Hybrid Coordinate Ocean Model with the Navy Coupled Ocean Data Assimilation (HYCOM-NCODA) with a 1/12° horizontal resolution, and GLORYS2V3 and FOAM, both with a 1/4° horizontal resolution. These Ocean Forecasting and Analysis Systems (OFAS) are able to capture the mean observed features in the 22° S region, showing a BC core confined to the west of 39° W and an Intermediate Western Boundary Current between the depths of 200 and 800 m. However, the OFAS tend to overestimate the mean BC baroclinic volume transport across the AX97 reference transect and underestimate its variability. The OFAS show that the coastal region between the coastline and the western edge of the AX97 transect plays an important role in the mean BC total transport, contributing to up to 23 % of its value, and further that this transport is not sampled by the XBT observations with its current sampling strategy. In order to understand the variability of the BC, a statistical classification of the BC is proposed, with the identification of three different events: weak, intermediate, and strong.

Responsible Editor: Pierre De Mey

This article is part of the Topical Collection on *Coastal Ocean Forecasting Science supported by the GODAE OceanView Coastal Oceans and Shelf Seas Task Team (COSS-TT)*

✉ Mateus O. Lima  
matdolima@gmail.com

- <sup>1</sup> Graduate Program in Geophysics, Federal University of Bahia (UFBA), Salvador, Brazil
- <sup>2</sup> Oceanographic Modeling and Observation Network (REMO), Rio de Janeiro, Brazil
- <sup>3</sup> Institute of Geosciences, Federal University of Rio de Janeiro (UFRJ), Rio de Janeiro, Brazil
- <sup>4</sup> Institute of Oceanography, Federal University of Rio Grande (FURG), Rio Grande, Brazil
- <sup>5</sup> Physical Oceanography Division, Atlantic Oceanographic and Meteorological Laboratory, National Oceanic and Atmospheric Administration (NOAA/AOML), Miami, FL, USA
- <sup>6</sup> Cooperative Institute for Marine and Atmospheric Studies, University of Miami, Miami, FL, USA

**Keywords** Western Boundary Current · Brazil Current · Ocean Forecast and Analysis Systems · AX97 reference transect · XBT

## 1 Introduction

The Brazil Current (BC) is the Western Boundary Current (WBC) that flows southward, adjacent to the Brazilian continental margin, and closes the South Atlantic Subtropical Gyre. Long period variability of the gyre and its associated currents has been hypothesized to be linked to changes in the Atlantic Meridional

Heat Transport and interbasin exchanges (Zhao and Johns 2014). As the BC flows along the Brazilian continental margin, it shows a very distinct vertical structure and mesoscale activity. Between 20° S and 28° S, it can be described as a warm and saline southward flow that ranges from the surface to depths of 400–550 m (Stramma and England 1999). The BC transports two water masses, the Tropical Water at surface levels and the South Atlantic Central Water (SACW) at pycnocline levels. Underneath the BC, the Intermediate Western Boundary Current (IWBC) flows northward along the continental slope and has a vertical extension of at least 700 m (Stramma and England 1999). According to these studies, the southward-flowing Deep Western Boundary Current (DWBC) may occupy the bottom 2 km of the water column. Within the previously mentioned latitudinal range, the vertical structure of the BC system presents a singular regime in terms of subtropical WBC, while its width ranges from 100 to 120 km and has a maximum surface speed of 0.4 to 0.7 m/s (Silveira et al. 2008). Despite its relatively low maximum velocity, the BC system is associated with intense mesoscale activity, particularly in the Brazil-Malvinas Confluence region, exhibiting strong year-to-year variability (Goni et al. 2011), shedding of large anticyclonic rings (Lentini et al. 2006), and possibly contributing to the low frequency variability of the South Atlantic meridional heat transport (Dong et al. 2015).

Near Cabo Frio (23° S), most of the studies of the BC volume transport have relied upon geostrophic computations (e.g., Signorini 1978; Campos et al. 1995; Silveira et al. 2000; Mata et al. 2012; Biló et al. 2014). Although these works are based on the use of different reference levels, results indicate that most of the BC geostrophic transport is confined to the first 200 m of the water column, and meanders and eddies were captured close to Cabo Frio (23° S). The BC southward transport from geostrophic estimates can reach values of  $5.6 \pm 1.3$  Sv at the Santos Basin (25° S to 27° S) (Biló et al. 2014). These estimates were based on different observations, including direct velocity measurement from current meter moorings to expendable BathyThermograph (XBT) data. Mata et al. (2012) used XBT data to estimate the mean BC baroclinic transport across 22° S using the AX97 XBT transect observations (Fig. 1) and found an average baroclinic transport value of 2.3 Sv west of 39° W. Transport measurements from current meter moorings (Müller et al. 1998; and more recently Rocha et al. 2014) verified the increase of the total transport, from 4.9 to 10.0 Sv, as the BC flows from 22° S to 28° S.

Despite the recent advances in understanding the BC mean flow, variability, and associated features, several aspects of the BC low latitude variability remain unexplained. The main reason for this is still the relative lack of synoptic observations. For instance, south of 18° S, the BC flow is mainly composed of eddies and, therefore, the average current transport is aliased by strong temporal and spatial fluctuations (Campos et al. 1995; Campos 2006; Soutelino et al. 2011). With the

goal of improving our understanding of the spatial and temporal variability of the BC, the high-density AX97 XBT transect was initiated in 2004 to measure the upper ocean temperature structure between Rio de Janeiro (22.9° S, 43° W) and Trindade Island (20° S, 30° W). The AX97 transect region (Fig. 1) is characterized by intense mesoscale activity; its variability has been linked to weather patterns in a region of great economic importance to Brazil (Mill et al. 2015) and is one of the longer-term monitoring systems of the BC.

Recommendations for the improvement of the current ocean observing system may be often addressed through the use of numerical models with data assimilation (Dotto et al. 2014). Ocean Forecasting and Analysis Systems (OFAS) provide a physical image of the global climate during the period in which available data exist, making it possible to minimize the lack of information in the spatial and temporal coverage in these regions. However, these systems can produce spurious biases and non-homogeneity caused by both numerical approximations and sampling limitations in data assimilation. Therefore, an evaluation of the adequacy, consistency, and applicability of these systems to long-term investigations of the BC is necessary.

The main goal of the present study is to evaluate the BC structure and variability at 22° S using observations from the high-density XBT AX97 transect, which are assessed against those obtained from three distinct OFAS. These models are made available within the framework of the *Global Ocean Data Assimilation Experiment (GODAE) Ocean View* and are used to add information to the XBT data on the main oceanographic features in the region. In order to reach this goal, two objectives are addressed: (a) the evaluation of the ability of the spatial-temporal design of the high-density AX97 transect to represent the BC average features and (b) the assessment of the different BC dynamic events identified by the XBT data.

## 2 Data and methods

### 2.1 Data sampled at the high-density AX97 XBT transect

Brazilian institutions, in partnership with NOAA, implemented the high-density XBT AX97 transect as part of the MOVAR (monitoring the upper ocean transport variability in the western South Atlantic) project. Therefore, the high-density XBT AX97 transect data will be referred as the MOVAR data. This project collects XBT data using Brazilian Navy opportunistic ships along a section that starts near Cabo Frio (Rio de Janeiro) and ends close to the Trindade Island (Fig. 1, grey lines). The data collection began in August 2004, and on average, it is carried out four times a year. In the present work, the study is limited to data obtained prior to 2012, which correspond to 37 realizations (cruises). The XBT sampling is performed with a typical horizontal spacing of 27 km along the transect, with the resolution increasing to 18 km near its borders. The vast majority of

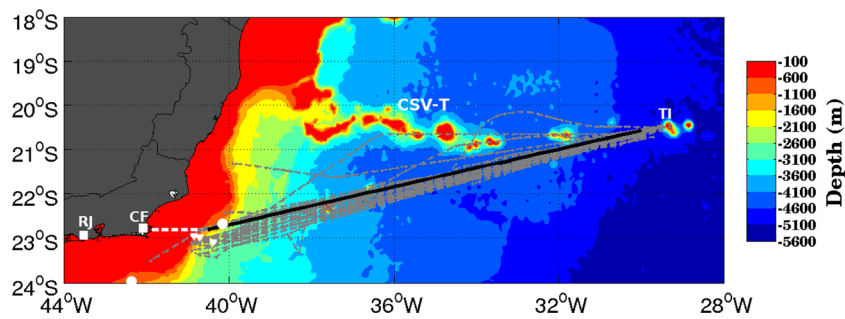


**Fig. 1** The AX97 transects with deployment positions (grey lines), the reference transect (black line), and the coastal transect (white dashed line). The Rocha et al. (2014) current profiles named MARLIM (22.7° S) and DEPROAS FBS (24.15° S) are indicated with white circles, and the three moorings used in Müller et al. (1998) are indicated with white

triangles. The main ship route goes from Cabo Frio City (CF) to Trindade Island (TI). The color shade represents the regional bathymetry (units in meters). The position of the Vitoria-Trindade Ridge (CSV-T) and Rio de Janeiro City (RJ) is indicated

samples used Sippican Deep Blue probes, which measure temperature profiles to approximately 800-m depth, with additional sampling carried out using Sippican T-5 probes, which measure temperature to 1830-m depth. XBT measurements are performed by sampling temperature and the elapsed time of descent of the XBT probes. The time of descent ( $t$  in seconds) is converted to depth ( $z$  in meters) using the standard manufacturer's fall rate equation (FRE) and following the new proposed corrections (Cheng et al. 2014). Using historical T-S relationships within a statistical scheme (Thacker 2007a, b), the salinity is estimated at gridded values of latitude, longitude, and depth, as a quadratic function of temperature. The use of the XBT data in this study leads to several sources of error. The most important of these errors are related to the temperature data precision, depth accuracy of the FRE, and salinity inference. Several authors analyzed and discussed typical error values (e.g., Goni and Baringer 2002; Thacker 2007a, b; Goes et al. 2013). For the temperature precision, according to the manufacturer (Sippican/Lockheed Martin), the XBT measurement error 0.1 °C and the maximum tolerance for the depth error associated with the FRE are approximately linear with depth, either 5 m or 2 % of depth. The Cheng et al. (2014) corrections reduce considerably the measurement errors. In addition, Cheng et al. (2014) concluded that these XBT errors did not affect the estimates of currents variability where the objective did not involve the assessment of long-term climate signals. The salinity error is derived from the Thacker 2007a, b methodology and was not calculated for the study area. Goes et al. (2013) found salinity error, at the central tropical Atlantic, of about 0.3 psu between in situ and climatological salinity estimates, resulting in dynamic height differences as large as 5 cm.

The first step in the data quality control was performed based on the temperature versus depth profile of each XBT deployment. A visual inspection of the temperature profiles was performed, in which profiles that contained strong systematic biases in comparison to their neighbors were removed. A five-point median filter was used to remove isolated spikes. After the pre-processing, data from each cruise were linearly interpolated to a

regular 10-m depth spacing and optimally interpolated along-transect to a 0.25° longitudinal spacing. The AX97 reference transect was adopted to eliminate, or at least reduce, the small scale and internal waves phenomena and to allow better direct comparisons between each transect sample. The latitude of the interpolated data was estimated on a line that connects Cabo Frio to Trindade Island (Fig. 1, black line). To calculate the baroclinic component of the geostrophic flow, the dynamical method was used for each pair of stations along the AX97 transect. Due to the scarcity of direct velocity measurements, we followed here the common practice to use the interface between superimposed currents of opposite flow as a level of no motion. Therefore, the depth of the  $\sigma_{\theta} = 26.8 \text{ kg/m}^3$  was used as reference level and was calculated for each cruise and each deployment. This density value is the level accepted as the typical interface between the BC southward flow and the IWBC northward flow (Pereira et al. 2014; Biló et al. 2014). The cross-section volume transport was estimated by the vertical integration of the regular grid in the AX97 reference transect (Mata et al. 2012).

Since the ageostrophic transport component may play an important role in the BC dynamics, the Ekman Transport was calculated using the *National Center for Environmental Prediction (NOAA/NCEP) Climate Forecast System Reanalysis (CFSR)*, with 1/4° horizontal resolution. We use this method to compare the total transport of the OFAS with the XBT baroclinic transport plus Ekman transport. Consequently, the role of the BC barotropic component can be analyzed in the OFAS, regarding the difference between the numerical and observation data.

To understand the oceanographic features in the study area, the new version of “Segment Sol multimissions d’Altimétrie, d’Orbitographie et de localisation précise”/ Developing Use of Altimetry for Climate Studies (SSALTO/DUACS) products distributed by Satellite Altimetry Data (AVISO), so-called DUACS 2014, released on April 15, 2014, is used. The AVISO Absolute Dynamic Topography (ADT) and the OFAS Sea Surface Height (SSH) are compared in each BC dynamic event identified by the XBT data.

**Table 1** OFAS description according to GODAE OceanView

| System                      | Ocean model and resolution   | Sea ice model                                       | Atmospheric forcing   | Assimilation method            | Data assimilated  | Period    |
|-----------------------------|--|---|---|--------------------------------|---|-----------|
| HYCOM (Bleck 2002)          | Exp. 19.1, 1/12° resolution, 32 hybrid vertical grid (Cumplings 2005)    | Community Ice Code (CICE) (Hunke and Lipscomb 2010) | Surface forcing 1 hourly CFSR, 0.3125° horizontal resolution, wind stress, wind speed, heat flux, and precipitation | NCODA (Cumplings 2005)         | T and S profiles (XBT, Fixed Buoy, Drifting Buoy, ARGO, CTD), altimetry, SST, Thermosalinograph, Ship SST, Buoy SST, AX97 high-density XBT reference line | 2004–2012 |
| GLORYS2V3 (Madec 2008)      | NEMOv3.1 (Madec 2008), ORCA025, 1/4° resolution, 75 levels vertical grid | LIM2  | Heat, momentum, and fresh water fluxes from ERA-interim   | SAM2 and 3D-VAR                | SLA (MyOcean SLA TAC), SST, T and S profiles (CORAV3.3), sea ice concentration (IFREMER/ CERSAT) AX97 high-density XBT reference line                     | 2004–2011 |
| FOAM (Blockley et al. 2014) | NEMO (Madec 2008), ORCA025, 1/4° resolution, 75 levels vertical grid     | Los Alamos CICE (Hunke and Lipscomb 2010)           | Met Office Global Atmospheric NWP model output (Davies et al. 2005)   | NEMOVAR (Mogensen et al. 2012) | SST, SLA, T, and S profiles (ARGO, Gliders, Buoys, Marine Mammals, XBT, CTD), Sea Ice concentration (OSI-SAF).  | 2004–2012 |

**Table 2** Cruises dates of the realization of the AX97 transects organized by event and the Brazil Current position for the MOVAR and the OFAS

|                     | Cruise date         | BC position         |    |    |    |          |    |    |    |
|---------------------|---------------------|---------------------|----|----|----|----------|----|----|----|
|                     |                     | Onshore             |    |    |    | Offshore |    |    |    |
|                     |                     | M                   | H  | G  | F  | M        | H  | G  | F  |
| Strong events       | 02/14 to 02/16/2006 |                     | NA | NA | •  | •        | NA | NA |    |
|                     | 12/11 to 12/14/2006 |                     | NA | NA | •  | •        | NA | NA |    |
|                     | 04/21 to 04/24/2007 | •                   | •  | NA | NA |          |    | NA | NA |
|                     | 02/14 to 02/16/2008 | •                   | •  | •  | NA |          |    |    | NA |
|                     | 04/10 to 04/13/2009 |                     | NA | NA | NA | •        | NA | NA | NA |
|                     | 10/14 to 10/16/2009 | •                   | •  | NA | NA |          |    | NA | NA |
|                     | 05/04 to 05/08/2010 | •                   | NA | NA | NA |          | NA | NA | NA |
|                     | 04/02 to 04/04/2012 | •                   | NA | NA | NA |          | NA | NA | NA |
|                     | 12/05 to 12/09/2012 |                     | NA | NA | NA | •        | NA | NA | NA |
|                     | Intermediate events | 02/17 to 02/20/2005 | •  | •  | NA | •        |    |    | NA |
| 06/30 to 07/02/2006 |                     |                     | •  | NA | •  | •        |    | NA |    |
| 08/16 to 08/18/2006 |                     | •                   | NA | NA | •  |          | NA | NA |    |
| 03/05 to 03/07/2007 |                     | •                   | NA | •  | •  |          | NA |    |    |
| 06/27 to 06/29/2007 |                     | •                   | •  | •  | •  |          |    |    |    |
| 06/11 to 06/13/2008 |                     | •                   | •  | •  | NA |          |    |    | NA |
| 08/19 to 08/21/2008 |                     | •                   | •  | •  | •  |          |    |    |    |
| 02/03 to 02/06/2009 |                     | •                   | •  | •  | •  |          |    |    |    |
| 06/21 to 06/23/2009 |                     | •                   | •  | •  | NA |          |    |    |    |
| 12/09 to 12/11/2009 |                     |                     | •  | •  | NA | •        |    |    |    |
| 12/02 to 12/05/2010 |                     | •                   | •  | •  | •  |          |    |    |    |
| 05/03 to 05/06/2011 |                     | •                   | NA | NA | NA |          | NA | NA | NA |
| 08/16 to 08/23/2011 |                     | •                   | •  | NA | •  |          |    | NA |    |
| 11/29 to 12/05/2011 |                     | •                   | •  | •  | NA |          |    |    | NA |
| 02/24 to 02/27/2012 |                     | •                   | •  | NA | NA |          |    | NA | NA |
| 06/07 to 06/10/2012 |                     | •                   | •  | NA | NA |          |    | NA | NA |
| 07/26 to 08/01/2012 |                     | •                   | •  | NA | •  |          |    | NA |    |
| 08/15 to 08/18/2012 | •                   | •                   | NA | •  |    |          | NA |    |    |
| 10/22 to 11/01/2012 | •                   | •                   | NA | •  |    |          | NA |    |    |
| Weak events         | 08/29 to 09/02/2004 |                     |    | •  | NA | •        | •  |    | NA |
|                     | 08/12 to 08/15/2005 | •                   | •  | •  | •  |          |    |    |    |
|                     | 02/25 to 02/28/2007 |                     |    | NA | •  | •        | •  |    |    |
|                     | 08/24 to 08/30/2007 |                     | NA |    | NA | •        | NA | •  | NA |
|                     | 04/17 to 04/19/2008 | •                   | •  | •  | •  |          |    |    |    |
|                     | 12/06 to 12/08/2008 |                     | NA | •  | •  | •        | NA |    |    |
|                     | 02/08 to 02/10/2011 |                     |    | NA | •  | •        | •  | NA | NA |
|                     | 06/13 to 06/15/2011 |                     |    | •  | •  | •        | •  |    |    |
|                     | 10/18 to 10/21/2011 | •                   | •  | NA | NA |          |    | NA | NA |

The letters M, H, G, and F represent MOVAR, HYCOM, GLORYS, and FOAM, respectively. NA indicates that a given event was not captured by a certain OFAS

## 2.2 OFAS

Two oceanic reanalysis and one analysis products available in the GODAE OceanView framework are used for comparison: the Hybrid Coordinate Ocean Model with the Navy Coupled Ocean Data Assimilation (HYCOM-NCODA), the Global

Ocean Physics Reanalysis GLORYS2V3 (hereafter GLORYS), and the Forecast Ocean Assimilation Model (FOAM), respectively. The main features determining the model's choice are (i) the data assimilation capacity, (ii) a spatial resolution capable of solving or allowing the mesoscale activity identification (1/4° or higher), and (iii) a time series that would

encompass the observed data spanning from 2004 to 2012 and that would provide daily outputs of the results. Details of the adopted systems are summarized in Table 1. It is important to note that HYCOM and GLORYS assimilate the high-density AX97 transect, although FOAM does not assimilate.

The HYCOM (Bleck 2002; [www.hycom.org](http://www.hycom.org)) employs hybrid vertical coordinates to numerically solve the primitive equations that control the ocean dynamics. The global reanalysis 19.1 experiment is configured for the global ocean with HYCOM 2.2 as the dynamical model. The reanalysis is atmospherically forced by the hourly NCEP/CFSR reanalysis data, with a horizontal resolution of  $0.3125^\circ$ , which includes the wind stress, wind velocity, heat fluxes, and precipitation. In the present work, this experiment encompasses the period of January 2004 until December 2012.

The NCODA scheme is an oceanographic version of the multivariate optimal interpolation technique broadly used in atmospheric operational forecasting systems. A complete description of the technique is given in Daley (1991).

The GLORYS reanalysis of the Mercator Ocean is based on the version 3.1 of Nucleus for European Modelling of the Ocean (NEMO) (Madec 2008) and in the ORCA025 configuration, with  $1/4^\circ$  horizontal resolution and variables spatial discretization using the C grid of Arakawa. The atmospheric conditions are prescribed for the model using the CORE bulk formulation. The forcing fields are originated from the ERA-Interim reanalysis products (Simmons et al. 2006). For data assimilation technique, the model uses the Kalman filter reduced multivariate technique, based on the formulation of “Singular Extended Evolutive Kalman Filter” introduced by Pham et al. (1998). Mercator Ocean has been using this method for a few years in different configurations of ocean models and it is called “Système d’Assimilation Mercator” version 2 (SAM2).

The global FOAM is a system of operational analysis and forecasting run daily at the Met Office, with the capability of modeling the deep ocean regimes and coastal areas (Blockley et al. 2014). The deep Ocean Forecasting System FOAM was radically revised during 2010 when it was adapted to use the model of the European Core for Ocean modeling as a dynamic core (NEMO; Madec 2008). The global configuration of the model is based on the configuration of ORCA025 developed by Mercator Océan (Drévillon et al. 2008). The FOAM system’s assimilation scheme is the NEMOVAR (Mogensen et al. 2012). NEMOVAR is a multivariate assimilation scheme, 3D-Var, “first guess appropriate time” that was developed specifically for NEMO (Blockley et al. 2014).

### 2.3 Methods used for OFAS evaluation

To verify how the models represent the main observed features along the AX97 reference transect, they are interpolated onto the reference transect location, where GLORYS and FOAM preserve their original horizontal resolution and HYCOM was

degraded to  $0.25^\circ$  horizontal resolution in order to compare to the others models and the MOVAR data. In addition, the model data include a zonal coastal transect extension that connects the western end of the AX97 reference transect to the vicinity of Cabo Frio (Fig. 1). This extension data allows estimating of the remaining of the transport along the shelf that is not sampled by the AX97 transect. The horizontal velocity components are rotated  $13^\circ$  counterclockwise in order to obtain the cross-sectional component of the velocity to the AX97 reference transect, while for the coastal transect the east–west ( $u$ ) and north–south ( $v$ ) components are maintained. The net volume transport is calculated from the vertical integration of the velocity across the coastal transect and the AX97 reference transect, using the  $\sigma_\theta=26.8$  as the isopycnal reference level. To compare with the MOVAR data, the estimated BC transports in the OFAS are averaged over the days of each AX97 realization from 2004 to 2012, with the exception of GLORYS, where the time series spans through the end of 2011.

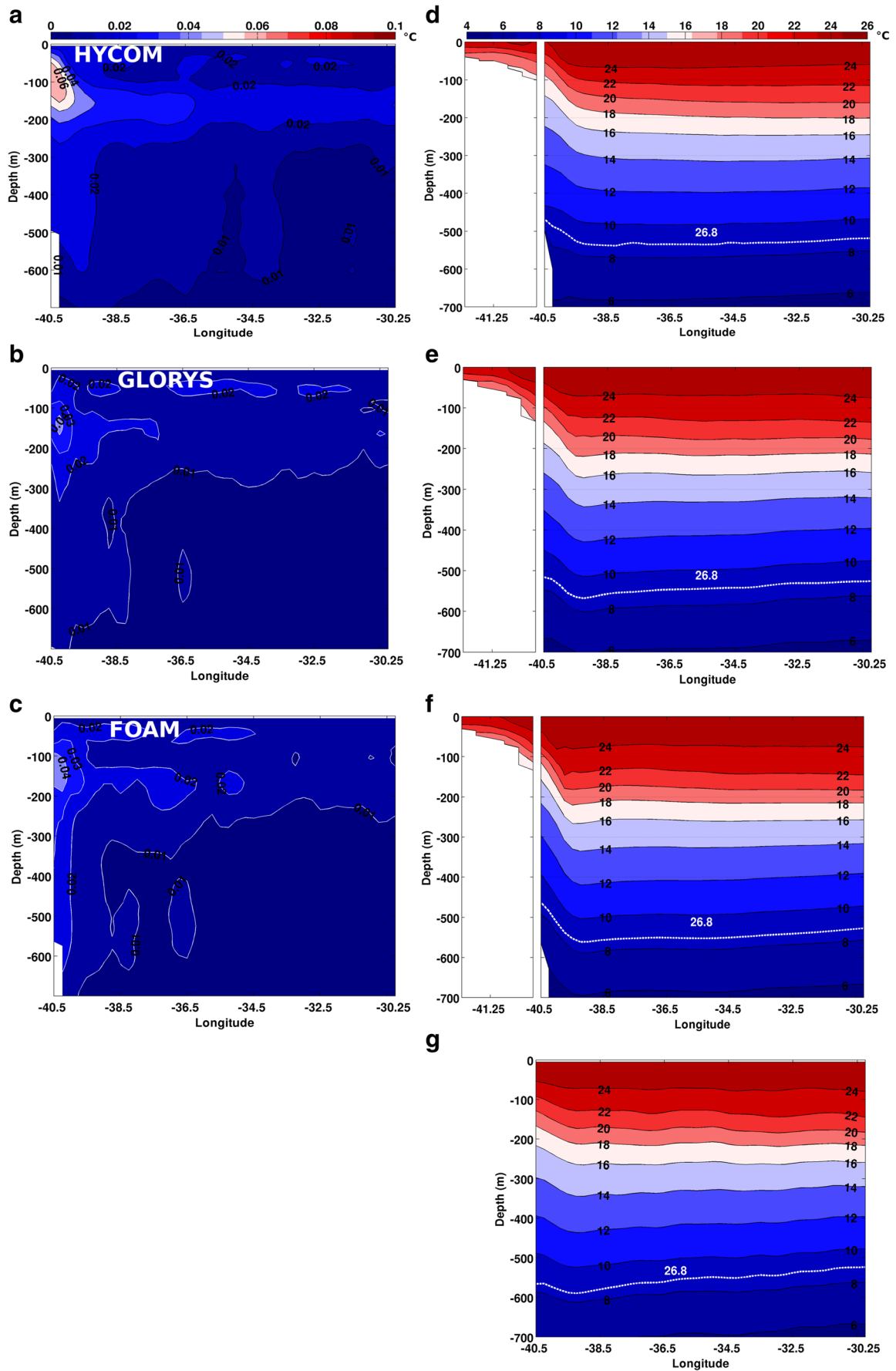
In order to compare the OFAS results with the XBT observations, the baroclinic velocity of the models is derived from the thermohaline structure using the dynamical method and the same isopycnal reference level ( $\sigma_\theta=26.8$ ), which varies for each time step and grid point. While the volume transport is also evaluated in the models for the total velocity field, this approach aims at reducing the error related to the assumptions to an arbitrary level of no motion and contributions from the ageostrophic motions.

Hereafter, the total velocity is referred to the velocity obtained from the OFAS outputs, and the baroclinic velocity is derived from the thermohaline structure of each data, using the dynamical method. The same definition is used for the volume transport. In the volume transport calculation, unless it is clearly stated, all calculations are based on net results. The positive (northward) and negative (southward) components of the volume transport are only used isolated to define the BC events.

### 2.4 The definition of BC events

The BC events are analyzed here in terms of different scenarios according to the BC intensity and the cross-shore position of its jet. For the different scenarios, two groups of events are established. The first group, which considers the strength of

**Fig. 2** Mean vertical distribution of the temperature ( $^\circ\text{C}$ ) root mean square error (RMSE) for the OFAS at the AX97 reference transect for the 37 XBT realizations (*left panels*) and mean vertical distribution of the temperature ( $^\circ\text{C}$ ) for the OFAS coastal transect and AX97 reference transect for the whole period (2004 to 2012) and MOVAR AX97 reference transect for the 37 XBT realizations (*right panels*). The OFAS are presented as follows: HYCOM (**a, d**), GLORYS (**b, e**), and FOAM (**c, f**). **g** Same distribution for MOVAR during the cruise periods. The mean depth of the  $\sigma_\theta=26.8 \text{ kg/m}^3$ , for each data, is represented by the *white dashed line*



the volume transport as an index, comprises the following events: (i) weak, (ii) intermediate, and (iii) strong. The second group considers the structure of the BC jet and is divided into the following: (i) close to the shelf break or (ii) offshore of the continental slope. The second group of events is used here to compare the intensity of the WBC with its position and to understand the causes of the displacement of the BC jet from the shelf break.

For the first criterion, the strength of the BC is evaluated based on the strength of the volume transport of the southward baroclinic flow between  $40.5^{\circ}$  W and  $39^{\circ}$  W. This longitude range was chosen as it comprises the mean BC dynamic core in all data sets. The BC southward baroclinic flow was used to define the events because, in this way, only the TW and SACW flow are evaluated. In order to provide a better assessment of the transport, the baroclinic volume transports obtained by both the OFAS and MOVAR are normalized.

The ranges to determine the intensity for each of the events are chosen based on the statistical distribution of the southward baroclinic transport values. The *strong* BC events are characterized by the highest 25 % of the volume transports of the BC. The *weak* BC events, on the other hand, encompass the cases falling within the 25 % lowest BC volume transports. The *intermediate* BC events include the remaining events lying in between these two events. For the OFAS, the limits between the BC events are calculated using the whole daily time series, while for MOVAR, only the 37 cruises data are used.

The second criterion, which is related to the cross-shore position of the BC, is based on the net BC baroclinic volume transport. Therefore, both the northward and southward cross-section velocities are included in the transport calculation. If the net cumulative baroclinic transport between the beginning of the AX97 reference transect ( $40.5^{\circ}$  W) and  $39.5^{\circ}$  W presents a northward component (positive values), the offshore event is defined; otherwise, the event is characterized as on-shore. Thus, the onshore event is well-defined if only southward (negative) transport values occur in the range of  $40.5^{\circ}$  W to  $39.5^{\circ}$  W.

For the comparisons between MOVAR and the OFAS, first, the BC events are identified in the observational data for each realization. Subsequently, in each model and for the time period of the 37 XBT transect realizations, the presence of the events defined by MOVAR is searched. Note that the percentile of the normalized transport of each OFAS (Fig. 10) was used in this search. Therefore, the OFAS may or may not find the same events defined by MOVAR. When the event is identified, the day selected within the time window of the XBT realization is the best match of the event in the models.

The 37 XBT transect realizations organized by their BC intensity events are shown in Table 2. The BC position in each realization and the capability of the OFAS to identify these events are also shown. A subsection in the “Results” section is

dedicated for this analysis, where one case study was selected to exemplify each event (strong, intermediate, and weak) characteristics and dynamic. The choice of the case studies was based first in the capability of the three models to identify the MOVAR event and then the same BC structure and dynamic in the four data sets. The strong BC event chosen was the XBT realization on February 14 to 16, 2008, for the HYCOM, GLORYS, and MOVAR, and the December 11 to 14, 2006, for the FOAM (Table 2). Only in this event, the models have different XBT realization date as the FOAM model was not able to capture the February XBT realization. The case study of the intermediate event was on 3rd to 6th of February 2009 and for the weak event was on 13th to 15th June, 2011 (Table 2).

## 3 Results

### 3.1 Temperature structure

The root mean square error (RMSE) between OFAS and MOVAR in the AX97 reference transect is shown in Fig. 2a–d. At the subsurface until 300-m depth at the longitude range of  $40.5^{\circ}$  to  $40^{\circ}$  W, all the models show a higher RMSE compared to the other regions. This region includes the mean BC core where the isotherms are steeper and the baroclinic flow is more intense. The mean temperature along the zonal coastal section and the beginning of the AX97 reference transect (Fig. 2d–g) show this pattern. Within the BC core, MOVAR (Fig. 2g) shows a less intense temperature (and density) horizontal gradients than the OFAS (Fig. 2d–f), which results in a less intense associated mean baroclinic velocity. HYCOM shows RMSE value of  $0.07^{\circ}$  C at the BC core, the highest among the models, and a RMSE range of  $0.03^{\circ}$  C to  $36.5^{\circ}$  W. GLORYS and FOAM present a similar RMSE in the mean BC core region, with values in the order of  $0.05^{\circ}$  C close to 150-m depth and  $40^{\circ}$  W.

Regarding the salinity structure, the RMSE between OFAS and the estimated climatological salinity in the AX97 reference transect (not shown) presents maximum values of 0.009 psu only. As the climatological salinity estimates are in a good agreement with the OFAS salinity, the difference between the baroclinic velocity of OFAS and MOVAR is probably related to the temperature structure.

The mean temperature along the zonal coastal section and the AX97 reference transect of models and MOVAR (Fig. 2d–g) show a vertical water mass distribution that is in agreement with previous results (temperature and salinity diagram not shown) (e.g., Campos et al. 1995). Warm Tropical Water can be observed approximately in the first 200 m of the water column in all OFAS and MOVAR. Further deeper and given the rate of temperature change in the thermocline, a temperature decrease to a value of  $9^{\circ}$  C is observed nearly 550 m. The

mean depth of the  $\sigma_\theta = 26.8$  isopycnal, which represents the interface between SACW and the upper part of the AAIW, is shown as a *white dashed line*. The thermocline waters can identify the SACW, and the AAIW mainly recognized by its characteristic salinity minimum (not shown) is around 1000 m (Boebel et al. 1997). All the data show this interface at approximately 500-m depth.

In general, all models were able to capture the mean isothermal structure of the 37 XBT realizations. The difference of isotherm slope given by the models against the MOVAR, at the beginning of the AX97 reference transect, is associated with the model configuration assimilation schemes and the still diffusive thermohaline configuration in the study area. As it will be discussed in the next section, this results in a

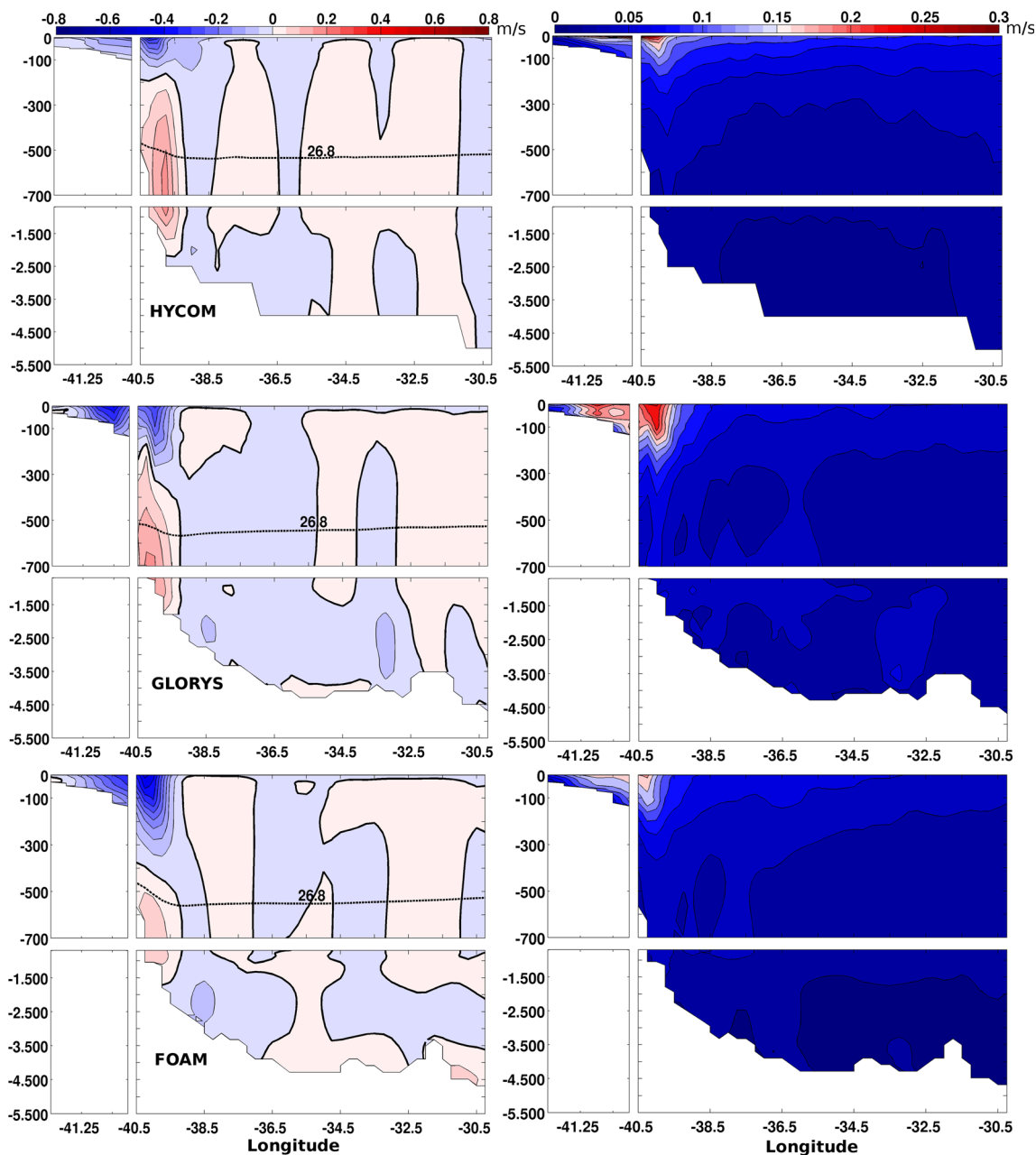


**Fig. 3** Mean cross-sectional component of the total velocity (*left panels*) and associated standard deviation (*right panels*) for the OFAS at both the coastal transect and the AX97 reference transect for the whole period (2004–2012). The OFAS are presented as follows: HYCOM (*upper panels*), GLORYS (*middle panels*), and FOAM (*lower panels*). Units are in meters per second, with negative (positive) values indicating a

southward (northward) flow. A *solid bold line* represents the zero contour of the velocity. The mean depth of the  $\sigma_\theta = 26.8 \text{ kg/m}^3$ , for each data, is represented by the *black dashed line*. The locations of the coastal transect and the AX97 transect are indicated in Fig. 1. The *horizontal scale* for the coastal transect is different from the AX97 reference transect

stronger horizontal gradient of mean dynamic topography for OFAS, which in turn produces a more intense baroclinic velocity.

### 3.2 Mean Brazil Current structure

In this section, we compare the total and baroclinic velocities of the BC between the models and MOVAR data and their associated transports. First, the velocity structure and the difference between the total and baroclinic velocity fields are assessed; second, the analysis of the BC volume transport is used to discuss the capability of the models to represent the

BC at the AX97 reference transect and then to analyze the BC transport components.

#### 3.2.1 Total and baroclinic velocities

Figures 3 and 4 show the total and baroclinic velocity fields averaged over the whole OFAS time series, respectively. The FOAM model (Fig. 3, third panel) shows the highest total velocity values of the BC core, approximately  $-0.47 \pm 0.19$  m/s. The easternmost limit of the mean region of BC influence in this model is  $39.25^\circ$  W, reaching depths up to 400 m. For the GLORYS model (Fig. 3, second panel), the BC maximum average velocity is approximately  $-0.32$

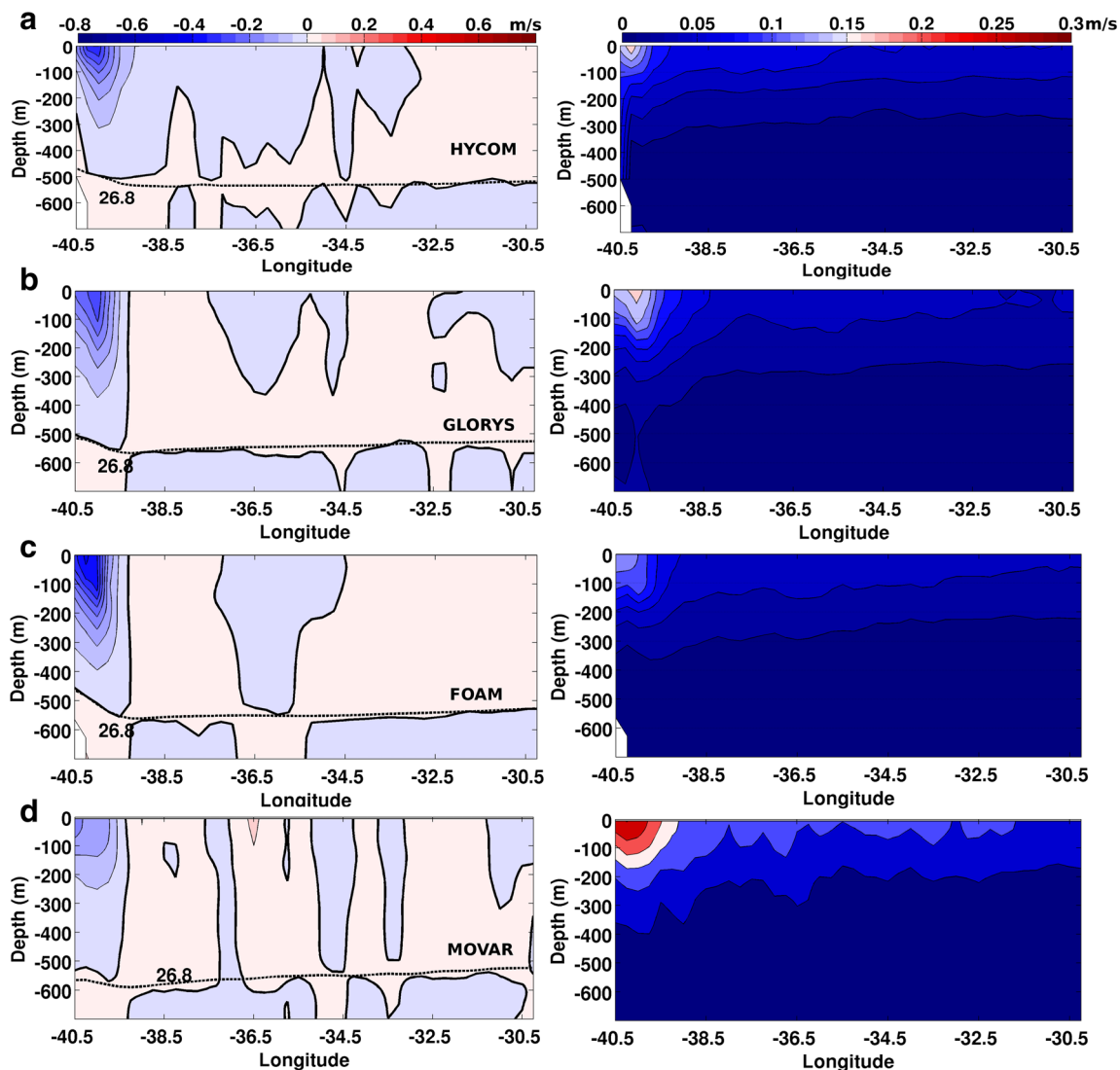


**Fig. 4** Mean cross-sectional component of the baroclinic velocity (*left panels*) and associated standard deviation (*right panels*) for the OFAS and MOVAR at the AX97 reference transect for the whole period (2004–2012). The OFAS are represented in the *vertical panels* from *top to bottom* in the following sequence: **a** HYCOM, **b** GLORYS, and **c** FOAM. **(d)** Same distribution for MOVAR during the cruise periods.

Units are in meters per second, with negative (positive) values indicating a southward (northward) flow. A *solid bold line* represents the zero contour of the velocity. The reference level of no motion is the  $\sigma_\theta = 26.8 \text{ kg/m}^3$ . A *black dashed line* in the *left panels* represents the mean depth of this isopycnal, for each data. The location of the AX97 transect is indicated in Fig. 1

$\pm 0.25$  m/s and the mean BC vertical limit is approximately 335-m deep at  $40^\circ$  W. GLORYS exhibited the less intense offshore BC among the OFAS and a double-core BC structure, where the coastal component of the BC is very intense, with negative values as large as  $-0.4$  m/s. HYCOM (Fig. 3, first panel) displays the shallowest BC, with the level of no motion shallower than 200 m, and a mean core velocity of  $-0.45 \pm 0.33$  m/s. The different OFAS BC total and baroclinic velocity are related to the many sources of uncertainty in ocean modeling (e.g., parameterized processes, initialization, atmospheric forcing, numerical implementation, data assimilation schemes, and vertical discretization, etc.) (Masina et al. 2015) (Table 1). As expected, HYCOM presents the highest variability, as a result of its increased original horizontal resolution.

An important aspect to be noted is the shallow level of no motion of HYCOM and GLORYS, in comparison to the interface between SACW and AAIW, represented by the depth of  $\sigma_\theta = 26.8$  isopycnal (Pereira et al. 2014; Biló et al. 2014). These two models present a total velocity structure not consistent with the observed thermohaline structure (Fig. 2), suggesting that the barotropic and non-Ekman ageostrophic velocity components could be a major source of error in these models. On the other hand, FOAM has a total velocity structure closer to the thermohaline structure, with the mean isopycnal level at similar depth range to the mean observed IWBC limit.

To better assess the capability of each OFAS to represent the mean dynamic structure of the BC against a more representative observational time and space series, the baroclinic

currents of the systems are calculated for the entire time series period and their mean fields are presented in Fig. 4. To be consistent with MOVAR, the OFAS baroclinic currents are calculated using the same methodology and isopycnal level. It is important to notice that the OFAS total velocity field (Fig. 3), although stronger, bears strong resemblance to the estimated baroclinic velocity fields of the XBT realizations (Fig. 4d).

The BC domain in all models and MOVAR is confined to the west of  $39^\circ$  W, with GLORYS (Fig. 4b) and FOAM (Fig. 4c) showing a similar mean pattern. For these two systems and also for the observed data, the BC is confined on average to the west of  $39.5^\circ$  W. HYCOM (Fig. 4a) is the OFAS that exhibited the largest WBC domain compared to the others systems, reaching longitudes of  $38^\circ$  W, although the BC core is limited to the west of  $39.5^\circ$  W.

With respect to the BC core velocity, MOVAR exhibits a maximum southward baroclinic velocity of  $0.17 \pm 0.30$  m/s (Fig. 4d). Other authors (e.g., Signorini et al. 1989; Campos et al. 1995; Mata et al. 2012) show similar values of baroclinic velocity for the region. The OFAS show a more intense BC than MOVAR. HYCOM and FOAM show similar mean BC core velocity of up to 0.4 m/s southward, whereas GLORYS values are closer to MOVAR ( $-0.29 \pm 0.17$  m/s). The steeper isotherms in the OFAS compared to MOVAR result in a stronger vertical shear that intensifies the horizontal pressure gradient and consequently the baroclinic BC velocity.

All models present a lower variability ( $0.17$  m/s for HYCOM, and  $0.14$  m/s for FOAM and GLORYS),

**Fig. 5** Mean cumulative depth integrated (surface to the depth of the  $\sigma_\theta = 26.8$  kg/m<sup>3</sup>) baroclinic volume transport (in Sv) along the AX97 reference transect. The vertical lines represent the associated standard deviation. For OFAS, represented in the following sequence, **a** HYCOM, **b** GLORYS, and **c** FOAM, the whole period is marked by black lines, while the period including only the MOVAR cruises is marked by red dashed lines. In panel **d** MOVAR baroclinic transport is marked by red dashed lines

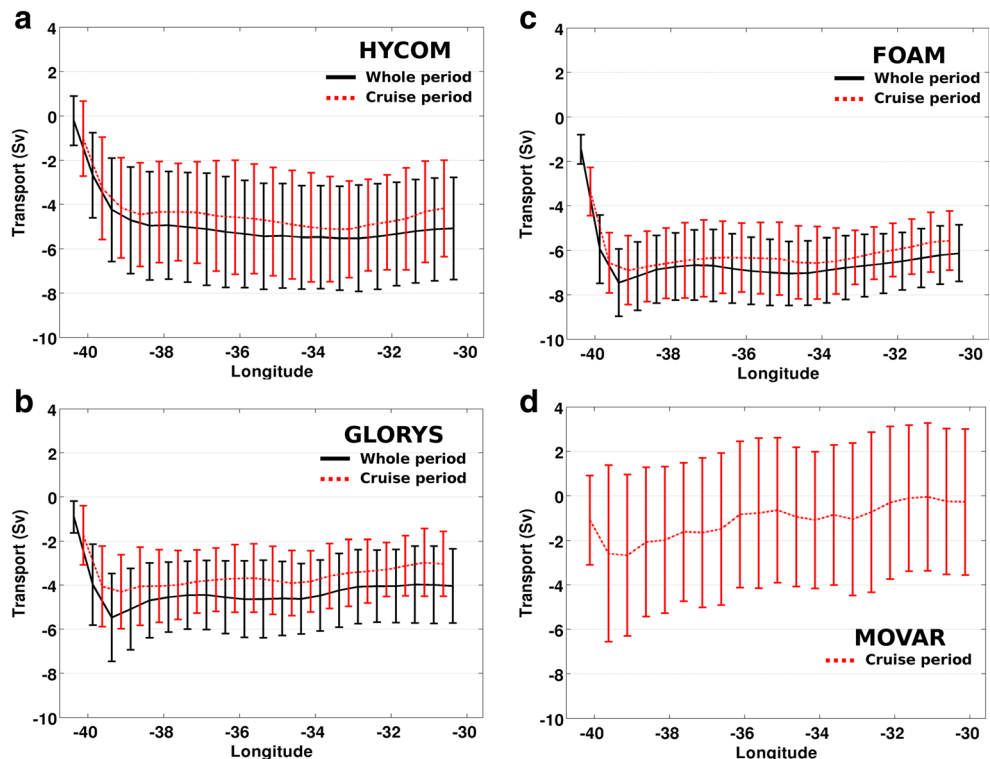
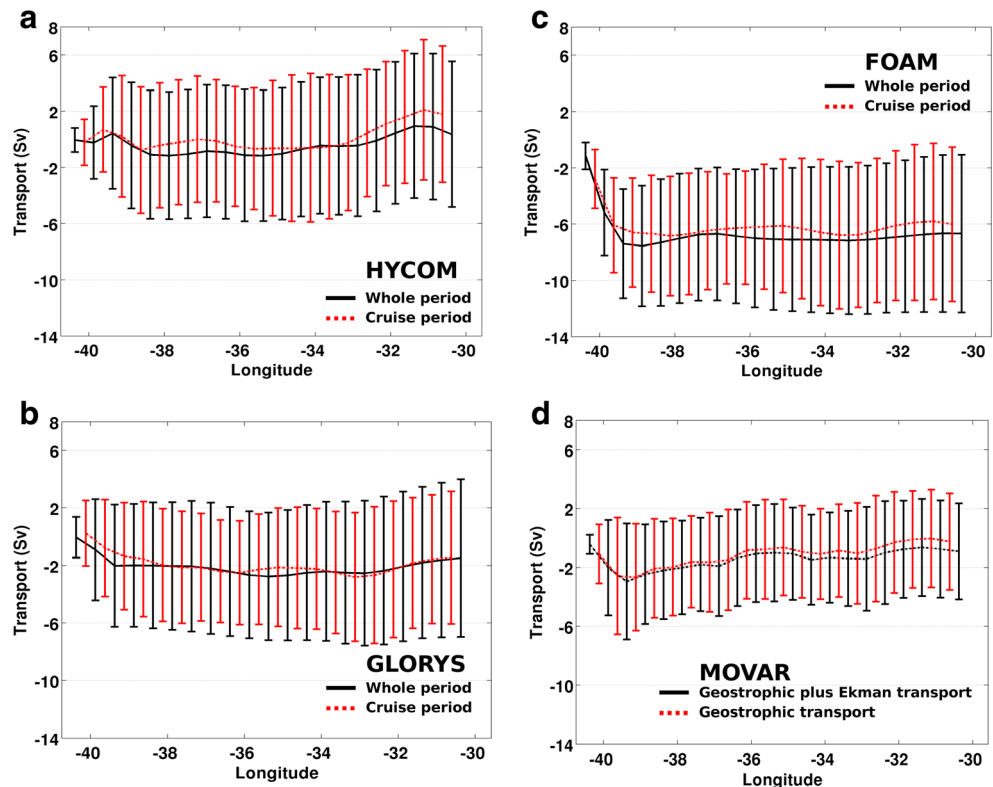


**Fig. 6** Mean cumulative depth integrated (surface to the depth of the  $\sigma_\theta = 26.8 \text{ kg/m}^3$ ) total volume transport (in Sv) for the AX97 reference transect. The vertical lines represent the associated standard deviation. For the OFAS, represented in the following sequence, **a** HYCOM, **b** GLORYS, and **c** FOAM, the whole period is marked by black lines, while the period including only the MOVAR cruises is marked by red dashed lines. In panel **d**, MOVAR mean cumulative depth integrated baroclinic volume transport presented in Fig. 5d is repeated for comparison purposes (red lines), whereas black lines mark this value plus the Ekman transport



approximately half of the BC velocity standard deviation (Fig. 4, right panels) shown in the observations ( $0.30 \text{ m/s}$ ). Model resolution may play a role in this discrepancy, since HYCOM without degradation, with a  $1/12^\circ$  horizontal resolution, shows a standard deviation of  $0.31 \text{ m/s}$  (not shown). However, results suggest that these models are still diffusive at this region, even in baroclinic terms.

While differences between observed and modeled results do occur, the analysis of the coastal transect velocity (Fig. 3) in conjunction with the MOVAR transect (Fig. 4) shows that the spatial sampling strategy of the XBT cruises was sufficient to represent the mean dynamics of the MOVAR transect. A quantification and discussion of the relevance of this coastal transect will be presented in the last part of the next subsection.

### 3.2.2 Baroclinic, Ekman, and total transports and the role of the continental shelf

In order to better assess the differences between the OFAS and MOVAR, the cumulative baroclinic transport, from west to east and from the surface down to the  $\sigma_\theta = 26.8$  isopycnal level, across the MOVAR reference transect is evaluated (Fig. 5). HYCOM shows a mean baroclinic transport at  $39^\circ \text{ W}$  of its entire time series (cruise period) of  $-4.7 \pm 2.4 \text{ Sv}$  ( $-4.5 \pm 2.3$ ). GLORYS presented similar values to HYCOM

along the MOVAR reference transect,  $-5.5 \pm 2.0$  for the whole period ( $-4.3 \pm 1.7$ , cruise period) Sv at  $39.5^\circ \text{ W}$ . In the case of HYCOM (Fig. 5a), this transport keeps increasing approximately until  $33^\circ \text{ W}$  reaching  $-5.5 \text{ Sv}$ , which can be related

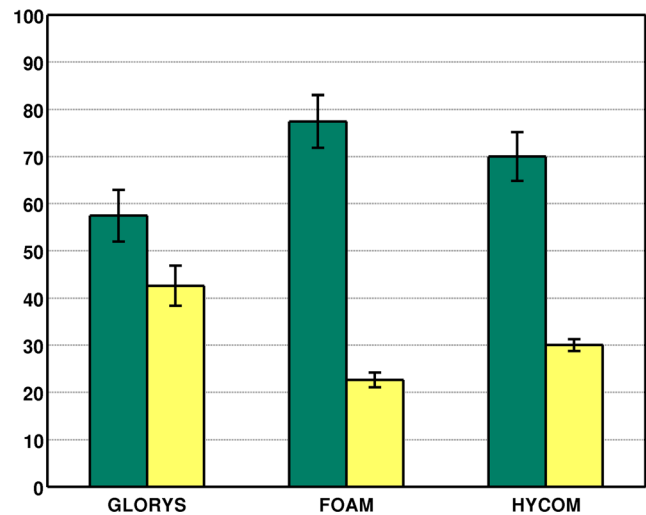


**Fig. 7** Percentage of the OFAS total depth integrated (surface to the depth of the  $\sigma_\theta = 26.8 \text{ kg/m}^3$ ) volume transport passing through the AX97 reference transect (green bar) and the coastal transect (yellow bar). The standard deviation is represented by the black vertical lines. The locations of the AX97 reference transect and coastal transect are indicated in Fig. 1

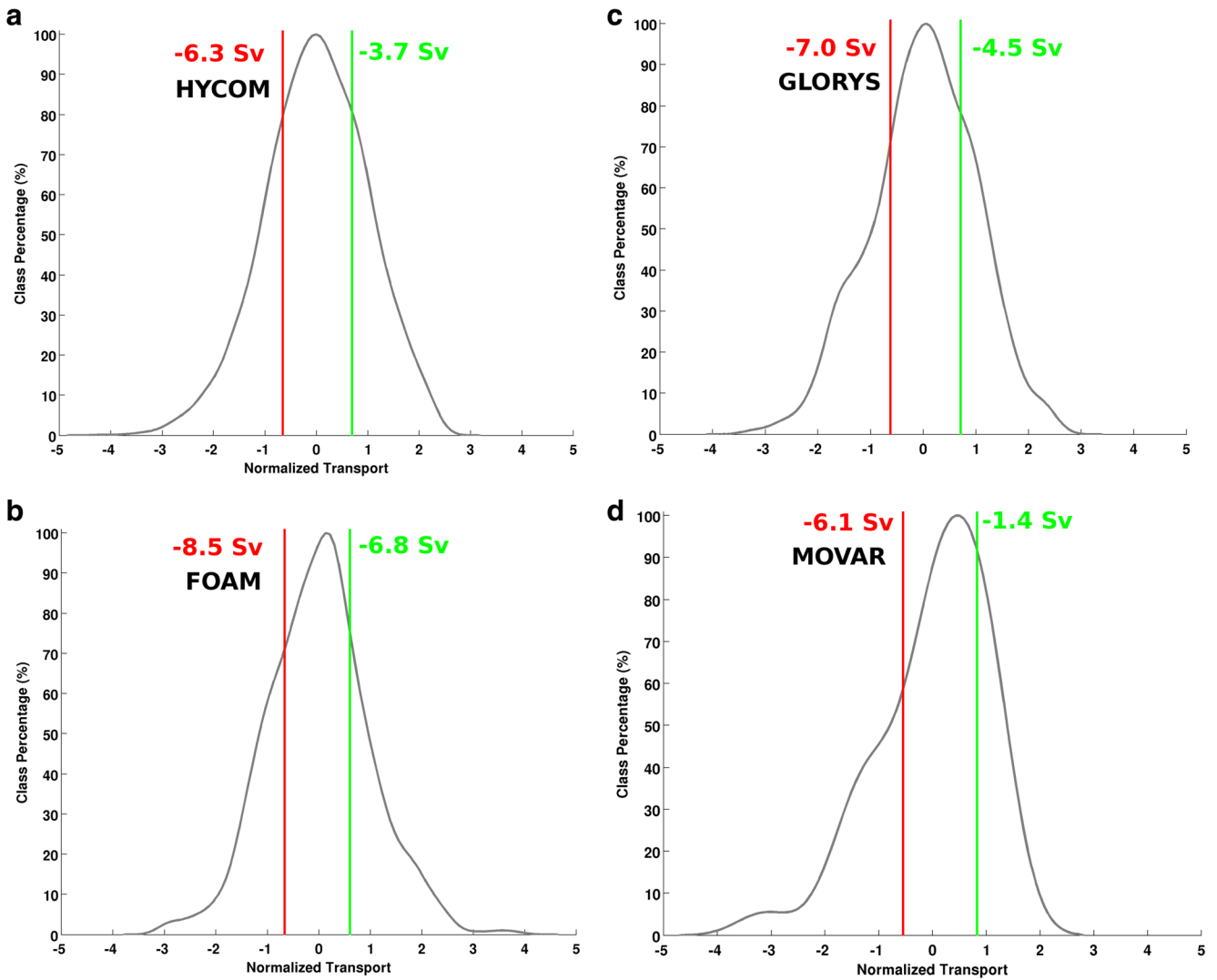
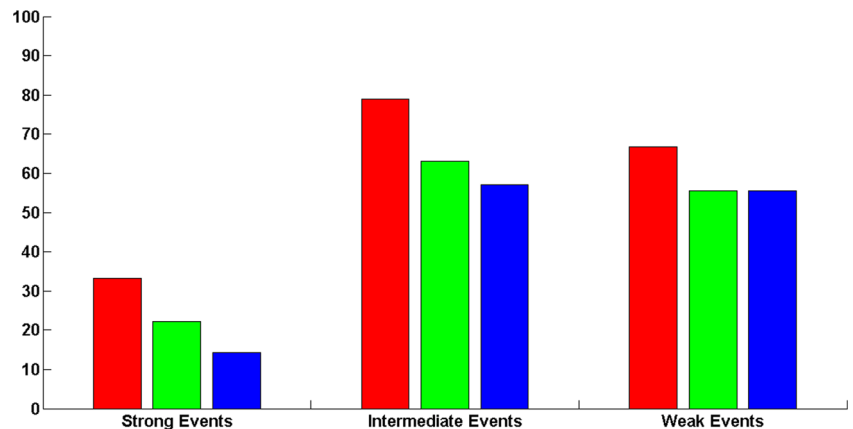


**Fig. 8** Normalized histogram of the depth integrated (surface to the depth of the  $\sigma_{\theta}=26.8 \text{ kg/m}^3$ ) baroclinic volume transport ( $T_n$ ) of the Brazil Current (considering only the southward transport) at the AX97 reference transect westward of  $39^\circ \text{ W}$ , for **a** HYCOM, **b** GLORYS, **c** FOAM, and **d** MOVAR. The descriptive events are divided in strong, intermediate, and weak events. The *green* and *red* lines represent the cutoff values for the weak and strong events, with the associated

volume transport for each OFAS and MOVAR. The *x* label is represented by the normalized transport  $\frac{T-\bar{T}}{\sigma}$ , where  $T$  is the baroclinic volume transport and  $\sigma$  is the standard deviation. The *y* label is represented by the percentage of each class related to the median, where 100 % is the median

**Fig. 9** Percentage of representation of the MOVAR events by the OFAS. The OFAS are indicated by the following colors: HYCOM (*red*), GLORYS (*blue*), and FOAM (*green*)



to its lower vertical resolution, as mentioned before. Among the OFAS, FOAM was the system with the most intense baroclinic transport, with a value of  $-7.4 \pm 1.5$  Sv ( $-6.9 \pm 1.5$ ) for the whole period (cruise period) for the same location. It is interesting to note that in the OFAS when only the cruise time periods are considered, the average BC transports estimated are weaker when compared to their mean whole time series transports. These results suggest that the XBT time sampling adopted may underestimate approximately 20 % of the baroclinic BC transport that crosses the MOVAR reference transect.

While the MOVAR baroclinic transport is smaller when compared to the OFAS, it is worth mentioning that the interpolation for the reference transect diminishes the BC transport. For instance, the baroclinic transport for the 37 XBT realizations at the MOVAR reference transect is  $-2.7 \pm 3.6$  Sv. When this transport is calculated for each cruise transect (Fig. 1, gray lines), this value increases to  $-2.9 \pm 3.6$  Sv. Therefore, the interpolation for a reference transect reduces the value of the mean transport, since the meridional velocity is weaker than the across transect velocity.

Figure 6 presents the total volume transport for the entire period at the MOVAR reference transect, whereas the values are associated to the BC at  $39^\circ$  W and the values in parentheses are associated with the same region but for the cruise periods only. FOAM (Fig. 6c) is the system with the largest BC transport, about  $-7.6 \pm 4.3$  Sv ( $-6.7 \pm 4.1$ ), followed by GLORYS (Fig. 6b) with a value of  $-2.0 \pm 4.2$  Sv ( $-1.6 \pm 4.0$ ). HYCOM (Fig. 6a) is the only model that presents a northward transport at the beginning of the MOVAR reference transect until  $39^\circ$  W, as a consequence of the shallow IWBC core that diminishes the integrated total transport in the region. The southward transport only appears after  $39^\circ$  W and is maximum at  $38^\circ$  W with  $-1.2 \pm 4.5$  Sv for the whole time series. Among the OFAS, GLORYS is the system with the closer volume transport values to the MOVAR baroclinic plus Ekman transport (Fig. 6d), which is  $-2.9 \pm 3.9$  Sv. Interestingly, at  $39^\circ$  W, the Ekman transport only increases the BC flow by 0.2 Sv or 6.9 % of the flow. This value increases to up 0.6 Sv if the entire MOVAR reference transect is considered.

BC integrated volume transport between 2 and 10 Sv is found in the literature for the study area (Signorini et al. 1989; Campos et al. 1995; Müller et al. 1998; Silveira et al. 2004; Mano et al. 2009; Mata et al. 2012; Rocha et al. 2014; Biló et al. 2014). Apart from FOAM, the total volume transport standard deviations of GLORYS and HYCOM, as well as the baroclinic transport of MOVAR, also show values greater than the mean, although the total velocity of the models does not exhibit the same pattern. Therefore, the influence of the IWBC on the BC behavior is strong in these two models, and the baroclinic instability between these two currents (Silveira et al. 2008) increases the BC variability in the MOVAR reference transect. These results show the important role of the BC

variability at the Cabo Frio Region. It is also evident from the total volume transport values that FOAM has a positive bias at the BC region when compared with MOVAR, reaching a value of up to 4.7 Sv even when the Ekman transport is included.

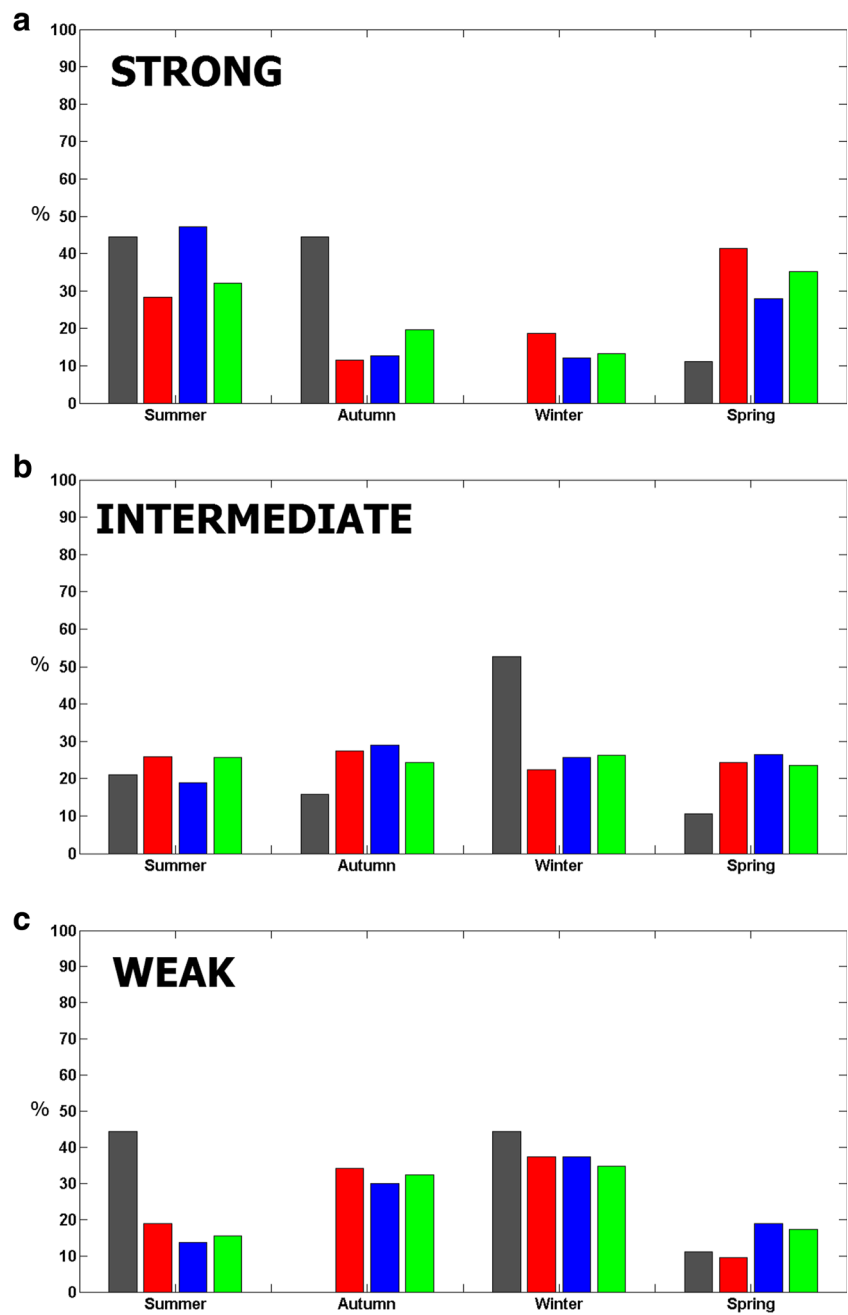
When comparing the OFAS and MOVAR, the difference is larger than the Ekman component, and the barotropic component may be the main cause, regardless of the additional uncertainties that were already discussed. According to Biló et al. (2014), the calculation of the BC velocity with only temperature profiling underestimated the barotropic component by 0.08 to 0.24 m/s compared with directly observed velocity field in the Santos Basin ( $25^\circ$  S to  $27^\circ$  S).

Finally, the role of the continental shelf in the BC dynamics and transport is also explored in the models. Figures 3 and 7 clearly show that part of the BC flows over the continental shelf across the zonal coastal transect in all of the OFAS. While the OFAS show a considerably higher portion of the transport passing through the MOVAR reference transect alone, varying between 77 % of the total mean transport for FOAM and 57 % for GLORYS, a significant portion of the flow can leak through the onshore region (Figs. 3 and 7). This amount is considerably higher in GLORYS ( $\sim 43$  % or  $-0.9 \pm 1.4$  Sv) because of its distinct double core BC structure. These results demonstrate that although the AX97 transect is able to cover a considerable percentage of the BC total volume transport (at least 57 %), it would be desirable to extend the high-density XBT AX97 transect toward the coast, encompassing the shelf and shelf break region.

### 3.3 Brazil Current events

Figure 8 shows the normalized histogram for the BC baroclinic transport (using only southward velocities) integrated until  $39^\circ$  W for the OFAS and MOVAR. All the OFAS show a symmetric distribution for the normalized histogram, whereas MOVAR shows an asymmetric distribution, where the median value is very distinct from the mean, and the transport values are skewed to the left, where the stronger BC transports occur. An essential question about the MOVAR normalized transport distribution is: are the 37 XBT cruises adequate to properly sample the BC strong event? Figure 8d indicates that the number of cruises carried out prior to December 2012 was not enough to identify the three BC behaviors, giving a low probability for the occurrence of a strong event. This is a solid indication that the AX97 XBT high-density transect has to be continued in order to homogenize the distribution of the current time sampling. Figures 5 and 6 also corroborate with this statement, since all OFAS show a smaller mean value for the cruise period when compared to the whole period, and the normalized transport histogram subsampled to the period of the cruises is asymmetric for all models (not shown).

**Fig. 10** Seasonality of the *strong* (a), *intermediate* (b), and *weak* (c) events for the MOVAR cruises (gray bar) and OFAS whole time series. HYCOM, GLORYS, and FOAM are indicated by the red, blue, and green bars



The percentage of representation by the OFAS of the observed events is indicated in Fig. 9. A representation of 100 % indicates that a given system was able to capture the totality of certain event. HYCOM is the OFAS that best represents all events compared to GLORYS and FOAM, where 80 % of the intermediate event is identified, 70 % of the weak event, and only 33 % of the strong event. GLORYS and FOAM better represent the intermediate and weak than the strong event. Since the BC is enhanced by mesoscale features near 22° S (Rocha et al. 2014) and the strong event is closely related to the current inversion near the 200-m isobaths, it is clear that the OFAS are not able to represent the BC mesoscale pattern at

the same spatial scales. Furthermore, GLORYS and FOAM are eddy permitting and, thus, do not resolve the ocean mesoscale features. In addition, because the coastal region is not used in the identification of the BC events, the statistics results have to be viewed with caution.

Several authors reported the meandering pattern of the BC and associated eddy formation around 22° S (Campos et al. 1995; Silveira et al. 2004; Silveira et al. 2008; Rocha et al. 2014), with velocity inversion close to the shelf break region. However, a more detailed description of the BC behavior in each of these events as well as a long time series to study them still does not exist for the BC.

In the following part of this work, an attempt to understand the major features and dynamic of each BC event is made, where one study case field of the baroclinic velocity and the associated integrated baroclinic transport, as well as the total transport, is presented for the AX97 reference transect for each event. In order to elucidate the regional aspects of the circulation, the mean SSH of the OFAS and the AVISO ADT for the selected study case are also described. For comparison purposes between the OFAS and AVISO, the mean value for SSH and ADT, considering the whole area presented in Figs. 11, 12, and 13a–d, has been removed. In addition, the BC axis position and seasonality are also discussed. It is important to note that AVISO is assimilated in the OFAS; thus, a similar pattern between the OFAS SSH and the AVISO ADT is expected to occur.

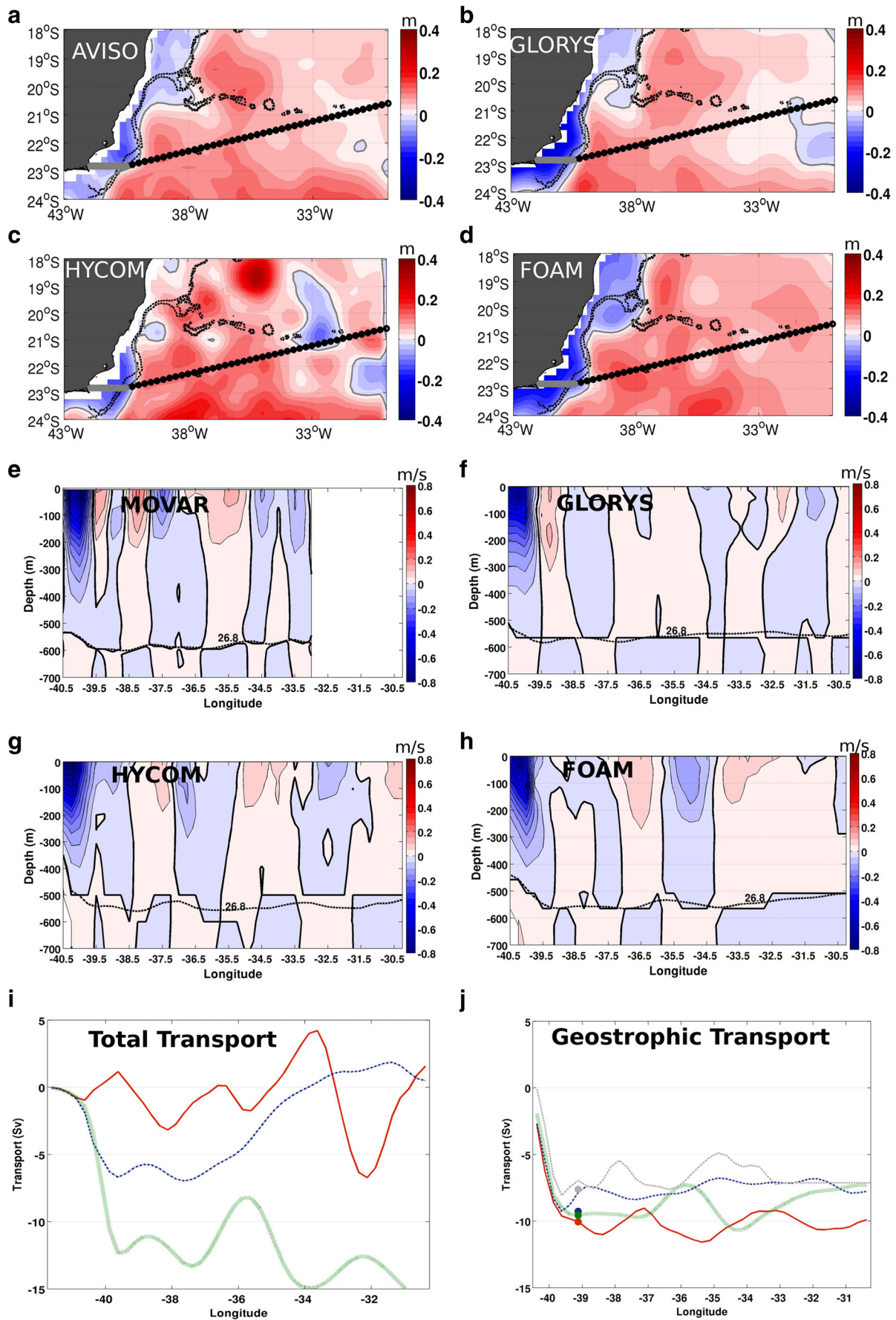
### 3.3.1 Strong events

For the nine strong events identified by MOVAR (Table 2), HYCOM identified three: FOAM captured two and GLORYS only one cruise. The study case presented in this section corresponds to the XBT realization of 14th to 16th of February 2008 (Table 2) for MOVAR, HYCOM, and GLORYS, and the 14th to 16th February 2006 for FOAM. The different XBT realization selected is due to the no representation of FOAM in the same date as HYCOM and GLORYS. Overall, the BC position in these strong events, for the XBT data, was located 44.4 % offshore and 55.6 % close to the continental slope (Table 2). The OFAS only represent onshore strong events; therefore, Fig. 10 does not show the BC inversion at the beginning of the AX97 reference transect. Due to the high percentage of offshore events, the meandering and eddies have a key role in increasing the BC volume transport.

In terms of seasonality (Fig. 10a), 44.4 % of the strong XBT cruise events occurred during the (austral) summer, 44.4 % in autumn, and only 11.2 % in the spring. Previous studies (Wainer et al. 2000; Goni and Wainer 2001) found that the transport associated with the BC is closely linked to seasonal variations in the local wind stress curl, and the BC intensified during the austral summer near the Brazil-Malvinas Confluence. Our results suggest that there is a latitudinal coherence in the seasonal variability of the BC. The use of daily outputs allows a comparison of the whole period of the OFAS time series. In this analysis, GLORYS shows the best results when compared to the XBT data seasonality, with summer being the season with the highest percentage of strong events (47.3 %), followed by the spring (27.9 %), autumn (12.6 %), and winter (12.2 %). For FOAM, summer and spring displayed similar percentages of 32 and 35.2 %, respectively. In the specific case of HYCOM, spring was the season with higher percentage of strong events (41.4 %), followed by summer with 28.3 %. These results reinforce that the BC strong behavior is predominantly in the summer in MOVAR,

**Fig. 11** A case study of a strong Brazil Current descriptive event: period of 14th to 16th of February 2008 (Table 2) for MOVAR, HYCOM, and GLORYS and the 14th to 16th of February 2006 for FOAM. **a** Mean absolute dynamic topography from AVISO and sea surface height for the OFAS, where **b** GLORYS, **c** HYCOM, and **d** FOAM. The gray (black) dots represent the coastal transect (AX97 reference transect). The dashed black lines are the 200- and 1000-m isobaths, and the gray line is the zero contour. Mean cross-section component of the baroclinic velocity for **e** MOVAR, **f** GLORYS, **g** HYCOM, and **h** FOAM at the AX97 reference transect. Units are in meters per second, with negative (positive) values indicating a southward (northward) flow. A solid bold line represents the zero contour of the velocity. The depth of the  $\sigma_\theta = 26.8 \text{ kg/m}^3$ , for each data, is represented by the black dashed line. **i** Cumulative depth integrated (surface to the depth of the  $\sigma_\theta = 26.8 \text{ kg/m}^3$ ) total volume transport (in  $\text{Sv}$ ) for the OFAS along the coastal and AX97 reference transects and **j** baroclinic volume transport for the MOVAR and the OFAS along the AX97 reference transect. For panels **i** and **j**, the colors represent MOVAR (gray), GLORYS (blue), HYCOM (red), and FOAM (green). The dots in **j** represent the BC southward component of the baroclinic volume transport for MOVAR and the OFAS

GLORYS, and FOAM. During the selected strong events, the ADT (Fig. 11a) and SSH (Fig. 11b–d) maps show a strong gradient near the 1000-m isobath at the beginning of the AX97 reference transect, with the sea level increasing eastward. This gradient strengthens the BC that flows adjacent to the 1000-m isobath to the west of  $39^\circ \text{ W}$ . For the OFAS, this gradient is even more intense than the observed data, especially for GLORYS and FOAM, which intensify the high-sea-level “cell” in the AX97 region for all OFAS. This high-sea-level cell is part of double-cell structure at the western end of the South Atlantic Subtropical Gyre (SASG) (Mata et al. 2012). This feature is well described in the mean surface circulation obtained by gravimetric mission GRACE satellite (Vianna et al. 2007) and also by satellite altimetry (Vianna and Menezes 2011). Another remarkable feature in Fig. 11 is the strong meander pattern of the BC as the flow goes southward. In the AVISO ADT map (Fig. 11a), it is clearly the BC bifurcation across the Vitoria-Trindade Ridge (CSV-T) at  $20.5^\circ \text{ S}$  and a strong meandering close to  $20^\circ \text{ S}$ . These results corroborate the study of Evans and Signorini (1985) which described that the BC along the poleward path trifurcates when it crosses the CSV-T. More recently, Mata et al. (2012) reported that the larger portion of the BC turns eastward in some instance, crossing the ridge in eastern channel and then turning back to the west, where it joins the weaker western portion further south. The meander is also present in all OFAS events close to  $19^\circ \text{ S}$ . HYCOM exhibits an anti-cyclonic eddy detached from the current jet in a position more eastward than the other data. Probably due to the strong baroclinicity and topographic effects, the BC presents an energetic pattern with frequent formation of strong cyclonic and anticyclonic meanders south of the CSV-T (Campos 2006). This event in FOAM (Fig. 11d), which is in a different period, has similar SSH



dynamic features. Close to the shelf break between 20° and 21° S, the meandering pattern is similar to the Vitória eddy formation and growing (Schmid et al. 1995), and further south, close to the AX97 reference transect, the meandering BC is due to the Cape São Tomé cyclonic meander. Thus, the strong event, study here, is characterized by a meandering current that could release eddies (Fig. 11c), along the Brazilian coast and a strong gradient at 22.5° S (Calado et al. 2006; Silveira et al. 2008), which is also related to the high-sea-level cell position and intensity.

The associated mean baroclinic velocity at the AX97 reference transect for the strong event is presented in Fig. 11e–h. OFAS and MOVAR show the BC domain confined in 39° W and close to the shelf break. BC velocities more intense due to the presence of meanders and eddy have been verified by other authors (Silveira et al. 2004; Rocha et al. 2014). The BC baroclinic velocity is more intense than 0.6 m/s in all data, with MOVAR and HYCOM presenting similar values, in the order of 0.7 m/s. The total vertically averaged transport across the coastal line and AX97 reference transect is shown in Fig. 11i. The FOAM (green line) exhibits the strongest BC, with a maximum intensity of  $-12.4$  Sv at 39.5° W, followed by GLORYS (blue line), and  $-6.7$  Sv HYCOM (red line) is the system with the least intense total transport for this study case, with 1.0 Sv at the beginning of the AX97 reference transect (40.5° W). HYCOM also shows a northward current at 39.5° W.

The baroclinic transport of MOVAR reaches a maximum intensity of  $-8.1$  Sv, whereas all OFAS present a more intense BC transport. The transport using only the southward component of the flow at 39° W, marked by the dots, exhibits very close agreement between the three OFAS. Interestingly, HYCOM shows the strongest BC transport, approximately  $-10$  Sv, which is due mostly to the reference level discrepancy.

### 3.3.2 Intermediate events

The intermediate events represented by 19 XBT cruises are best captured by HYCOM, where 15 cruises were identified, followed by 12 in FOAM and only eight in GLORYS. For this phase, the majority of the XBT cruises occurred during (austral) winter (52.6 %) (Fig. 10b), followed by summer (21.1 %), autumn (15.8 %), and spring (10.5 %). In a somewhat different fashion, the analysis of the OFAS daily outputs between 2004 and 2012 (Fig. 10b) does not display a clear seasonality in the BC intermediate behavior. The same seasonality distribution occurs in all systems, where each season represents around 25 % of the events.

The XBT cruises show that BC position was located close to the shelf break region in 89.5 % of this phase and only 10.5 % of the cruises exhibited a northward transport in the beginning of the AX97 reference transect, which is the

**Fig. 12** A case study of an intermediate Brazil Current descriptive event: period of 3rd to 6th of February 2009 (Table 2). **a** Mean absolute dynamic topography from AVISO and sea surface height for the OFAS, where **b** GLORYS, **c** HYCOM, and **d** FOAM. The *gray (black)* dots represent the coastal transect (AX97 reference transect). The *dashed black lines* are the 200- and 1000-m isobaths, and the *gray line* is the zero contour. Mean cross-section component of the baroclinic velocity for **e** MOVAR, **f** GLORYS, **g** HYCOM, and **h** FOAM at the AX97 reference transect. Units are in meters per second, with negative (positive) values indicating a southward (northward) flow. A *solid bold line* represents the zero contour of the velocity. The depth of the  $\sigma_\theta = 26.8$  kg/m<sup>3</sup>, for each data, is represented by the *black dashed line*. **i** Cumulative depth integrated (surface to the depth of the  $\sigma_\theta = 26.8$  kg/m<sup>3</sup>) total volume transport (in Sv) for the OFAS along the coastal and AX97 reference transects and **j** baroclinic volume transport for the MOVAR and the OFAS along the AX97 reference transect. For panels **i** and **j**, the colors represent MOVAR (*gray*), GLORYS (*blue*), HYCOM (*red*), and FOAM (*green*). The *dots* in **j** represent the BC southward component of the baroclinic volume transport for MOVAR and the OFAS

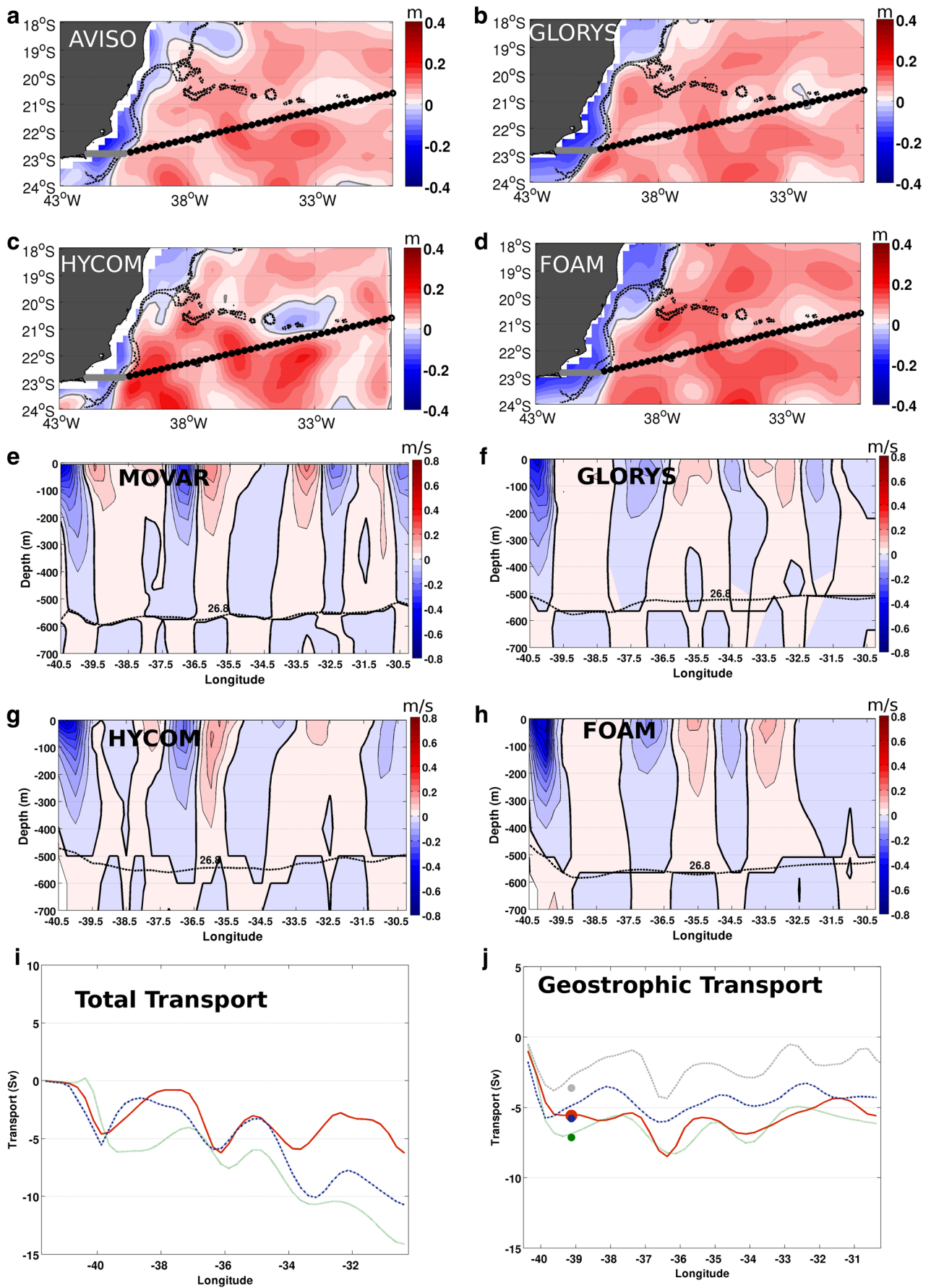
offshore BC position. Table 2 shows that the OFAS, with only a few exceptions, were able to identify the position of the current similar to the XBT data. This pattern is shown in all baroclinic velocity and transport panels (Fig. 12) of the models and MOVAR.

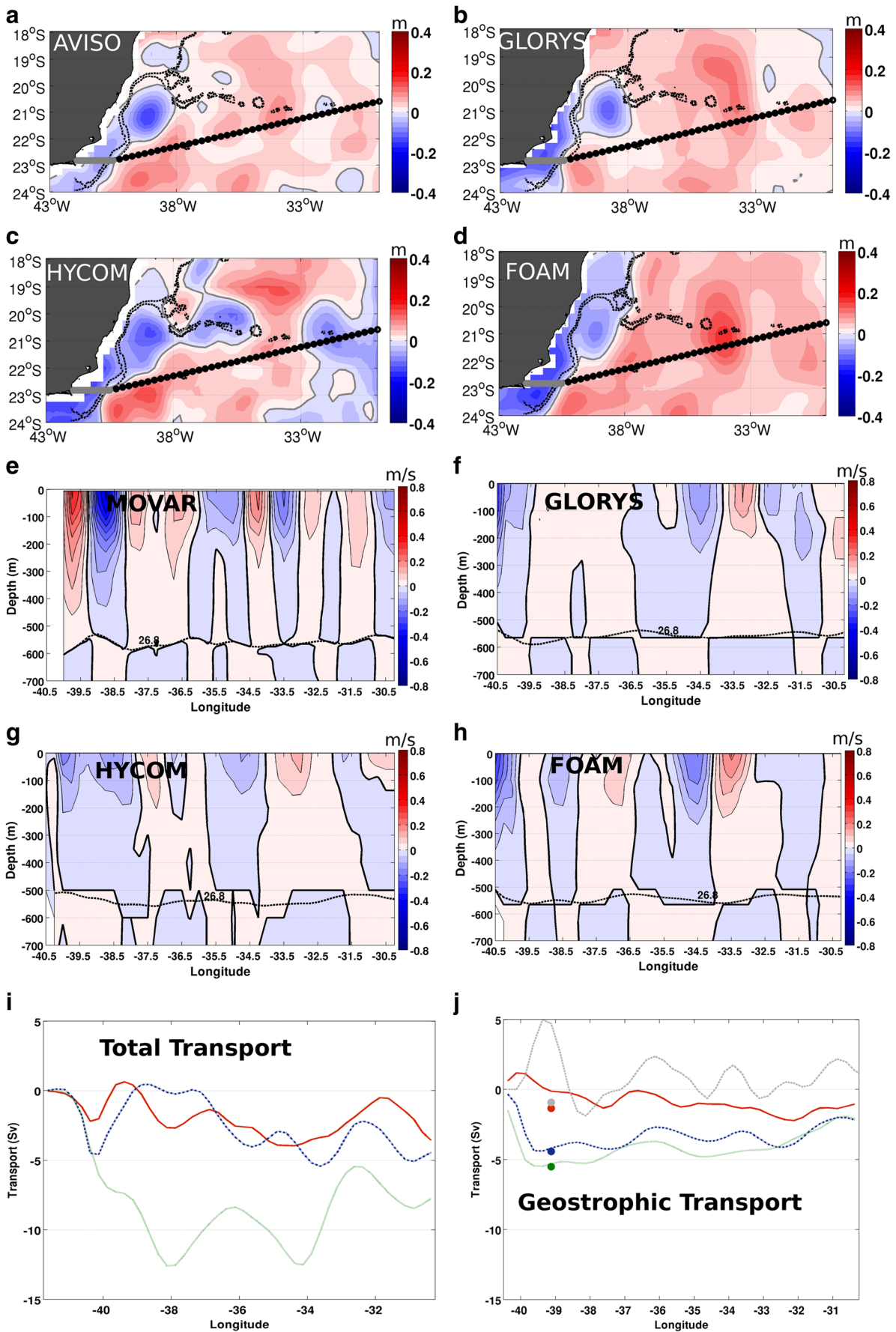
The AX97 section of 3rd to 6th of February 2009 (Table 2) has been chosen to characterize the intermediate events. As expected, the ADT (Fig. 12a) and SSH (Fig. 12b–d) maps exhibit a less intense BC, marked by weaker gradients of sea level elevation in both the OFAS and AVISO. The BC jet is located very close to the shelf break and confined in the beginning of the AX97 reference transect (Fig. 12e–h). The meander pattern observed in the strong event is not present in this event. The positive elevations of the sea level are still present and comprehend the entire AX97 transect characterized by the high-sea-level cell identified by Tsuchiya (1985) and Vianna et al. (2007).

The mean baroclinic velocities (Fig. 12e–h) show a similar structure in MOVAR and OFAS, with the BC confined to the west of 39.5° W and southward velocities reaching up to 0.4 m/s in the current core.

In terms of the mean total volume transport (Fig. 12i), FOAM (green line) is the OFAS with the strongest BC,  $-6.2$  Sv at 39° W, while at the transport inflection longitude, the BC in GLORYS (blue line) has about  $-5.6$  Sv, and in HYCOM only  $-4.6$  Sv. The coastal transect, mainly for HYCOM and GLORYS, represents a significant part of this transport,  $-0.6$  and  $-1.6$  Sv, respectively, while for FOAM, this value is  $-0.1$  Sv.

At the AX97 reference transect, the vertically averaged baroclinic transport in the OFAS (Fig. 12j), although more intense, follows closely the structure of the one derived from MOVAR. The baroclinic component of the BC in this event is stronger than the barotropic and ageostrophic terms. When only the southward component of the flow is analyzed, the OFAS also tend to intensify the BC when compared to the observed data.





◀ **Fig. 13** A case study of a weak Brazil Current descriptive event The Brazil Current descriptive event: period of 13th to 15th of June 2011 (Table 2). **a** Mean absolute dynamic topography from AVISO and sea surface height for the OFAS, where **b** GLORYS, **c** HYCOM, and **d** FOAM. The *gray (black)* dots represent the coastal transect (AX97 reference transect). The *dashed black lines* are the 200- and 1000-m isobaths, and the *gray line* is the zero contour. Mean cross-section component of the baroclinic velocity for **e** MOVAR, **f** GLORYS, **g** HYCOM, and **h** FOAM at the AX97 reference transect. Units are in meters per second, with negative (positive) values indicating a southward (northward) flow. A *solid bold line* represents the zero contour of the velocity. The depth of the  $\sigma_\theta = 26.8 \text{ kg/m}^3$ , for each data, is represented by the *black dashed line*. **i** Cumulative depth integrated (surface to the depth of the  $\sigma_\theta = 26.8 \text{ kg/m}^3$ ) total volume transport (in Sv) for the OFAS along the coastal and AX97 reference transects and **j** baroclinic volume transport for the MOVAR and the OFAS along the AX97 reference transect. For panels **i** and **j**, the colors represent MOVAR (*gray*), GLORYS (*blue*), HYCOM (*red*), and FOAM (*green*). The *dots* in (**j**) represent the BC southward component of the baroclinic volume transport for MOVAR and the OFAS

### 3.3.3 Weak events

The weak events are best identified by HYCOM, with 66.7 % of the cruises, whereas GLORYS and FOAM recognized 55.6 % (Fig. 9). Most of the nine XBT realizations that presented a weak BC occurred during (austral) winter and summer (44.5 %), followed by 11 % in the spring (Fig. 10c). For the OFAS time series, it is the winter that shows the majority of weak events occurrence (35 %), followed closely by the autumn (30 %), and the summer only represents 15 % of the cruises. The different seasonality of the OFAS and MOVAR (Fig. 10c) is probably related to the continuous time series of the models, enabling the models to better capture the seasonality of the weak events, or the more intense BC transport limits for this event in the models (Fig. 8), which can act to change the seasonality pattern. The seasonality of the models corroborates the study of Goni and Wainer (2001) near the Brazil-Malvinas confluence that found weaker BC baroclinic transport in the austral winter.

The offshore BC position is predominant in this event (78 %) with the remaining 22 % of the XBT realization showing the BC position onshore, close to the shelf break. HYCOM better represents the position of the BC jet compared to the others models (Table 2). GLORYS and FOAM poorly recognize the offshore position of the current jet.

The case study shown for this event is for the cruise realization of 13th to 15th of June 2011, where MOVAR and HYCOM presented an offshore BC current, and GLORYS and FOAM an onshore jet.

All the OFAS SSH (Fig. 13c–d) are very similar to the AVISO ADT (Fig. 13a), with a slightly trend to intensify the gradient in the BC jet. The high-sea-level cell is weaker in this event on the AVISO ADT, which decrease the BC intensity. All data show a cyclonic eddy centered at 21° S with an associated sea level drop, of at least 10 cm (14 cm for

AVISO data). This feature agrees with the eddies formed at Cape São Tomé (Mill et al. 2015) and is related to the velocity inversion at the beginning of the AX97 reference transect in MOVAR and HYCOM data (Fig. 13e, g, i). The same cyclonic eddy is observed in the other XBT realization (not shown). It is possible to conclude that the strong and weak events are related to the meander and eddy formation and growth close to the BC jet, where the position of the eddy influences the BC intensity. When the cyclonic eddy is close to the AX97 reference transect, at the vicinity or south of 21° S, the eddy decreases the baroclinic BC transport.

The baroclinic velocity (Fig. 13e–h) for the weak phase in MOVAR (Fig. 13e) presents a northward flow until 39.5° W related to the cyclonic eddy and a confined BC between 39.25° and 38° W. The core of the offshore BC was approximately  $-0.46 \text{ m/s}$ . HYCOM also displays a northward flow in the beginning of the AX97 transect at subsurface levels, and the BC is bifurcated with one core at 40° W ( $-0.2 \text{ m/s}$ ) and the other at 38.75° W ( $-0.12 \text{ m/s}$ ). FOAM and GLORYS presented a similar pattern with the BC confined to 39.5° W and a southward velocity of 0.3 m/s. In this case study, MOVAR presented the strongest BC. The mean total transport (Fig. 13i) shows that the coastal transect has a similar transport of  $-1.8 \text{ Sv}$  in GLORYS and FOAM, while the HYCOM-associated transport for this feature is less intense ( $-1.1 \text{ Sv}$ ). At the AX97 reference transect, the OFAS present a quite different pattern. While FOAM exhibits a more intense transport, reaching values of  $-12.6 \text{ Sv}$ , GLORYS and HYCOM are less intense,  $-4.6$  and  $-2.2 \text{ Sv}$  close to 40° W. Regarding the baroclinic transport, MOVAR shows a strong northward flow of  $4.9 \text{ Sv}$  as a consequence of the cyclonic eddy close to 21° S. HYCOM was the unique model that exhibits a northward transport, although less intense than MOVAR. FOAM and GLORYS show a similar BC baroclinic transport, approximately  $-3.5 \text{ Sv}$  at 39.5° W.

## 4 Discussion and conclusions

The main goal of this study is to assess the structure of the BC and its variability at 22° S, using data from the XBT AX97 transect, and three OFAS. The comparison between the observations and models can be used to identify major deficiencies on the ability of these products to represent the dynamics in the region and to recommend improvements in the sampling strategy along the AX97 transect. In addition, extreme events of the BC structure were identified and interpreted in terms of the regional dynamics.

Previous observational studies of the BC baroclinic structure often rely on assumptions about the level of no motion, in which the baroclinic velocities are referenced to. At the 22° S latitude, the accepted reference level is between the central (SACW) and intermediate (AAIW) waters, which lies

approximately along the  $\sigma_\theta = 26.8 \text{ kg/m}^3$  about 500 m deep (Pereira et al. 2014; Biló et al. 2014). Using this same assumption, the BC baroclinic core velocity and transport are estimated here from the XBT observations as  $-0.17 \pm 0.30 \text{ m/s}$  and  $-2.7 \pm 3.6 \text{ Sv}$ , respectively. In both cases, the variability (standard deviation) is larger than the mean. These results agree with previous observational estimates and show the important role of the mesoscale activity at  $22^\circ \text{ S}$ , associated with eddy formation and meander growth (Campos et al. 1995; Silveira et al. 2008; Mata et al. 2012; Rocha et al. 2014).

The three models analyzed (HYCOM, GLORYS, and FOAM) generally present a higher transport, and less variability of the BC when compared with the observations, due to the stronger temperature and dynamic height slope along the Brazilian coast. Regarding the greater variability in MOVAR, this data has, intrinsically, the entire energy of the flow summed up, including those scales smaller than  $0.25^\circ$ . Moreover, the models (HYCOM, GLORYS) show discrepancies with observations on the boundary between the Brazil and intermediate (IWBC) currents close to the depth of the  $\sigma_\theta = 26.8$  isopycnal, with the former much shallower ( $\sim 200 \text{ m}$ ) than the later ( $\sim 500 \text{ m}$ ). That fact tends to increase the baroclinic transport estimates in those models.

One aspect of the BC variability that is not sampled by the data is the along shelf transport. The models show that approximately 21 % of the BC transport flows along the shelf. In GLORYS, this can reach  $\sim 47$  % of the BC transport, although this model shows a two core BC mean structure that is not reproduced in the other models. Therefore, it is recommended that the AX97 transect extends its sampling closer to the coast ( $\sim 200\text{-m}$  depth).

When analyzing the BC transport values distribution for the MOVAR, it is observed a long tail for strong values, and the median skewed toward the lower values. This is not observed in the distributions as obtained from the models using their whole time period, whose results are more normally shaped. Therefore, another recommendation for the AX97 sampling is to extend time sampling, especially during austral autumn and summer, where stronger events of the BC transport generally occur. Indeed, in the models, the strong and weak BC transport events had a noticeable seasonality, with the strong events more in the summer, while the weak BC events are more frequent during winter.

We characterized the BC baroclinic transport in three types of events, relative to its southward transport strength along the beginning of the AX97 reference transect (between  $39^\circ \text{ W}$  and  $45^\circ \text{ W}$ )—weak, intermediate, and strong events—and discussed their main dynamic characteristics as observed from satellite SSH measurements. It is clear from the model outputs and the data that there is an association of strong and weak events with the mesoscale features in the region. For the strong event, in particular, there is a strengthening of the northern cell of the subtropical gyre, as well as the appearance

of the Cape São Tomé cyclonic meander (Calado et al. 2006; Silveira et al. 2008). In the weak events, the high sea-level gyre is located more to the South and the Cape São Tomé ring was present in the study case in early June 2011. The formation and northward displacement of this ring was analyzed in detail in previous works (e.g., Mill et al. 2015).

Regarding the BC position for the three events (weak, intermediate, and strong), when the current stays close to the shelf break, it is more frequently in the intermediate event, whereas the BC displacement offshore of the 1000-m isobath occurs more frequently during strong and weak events. The BC meandering and/or eddy formation can reverse the current locally, resulting in an increase or decrease of the transport of the current offshore of the 1000-m isobath (Silveira et al. 2008; Rocha et al. 2014). This current reversal is probably one of the most complex dynamical features captured by the OFAS.

We emphasize the importance of this and similar type of studies that conduct a direct comparison between numerical models and observations to infer the model structural errors, as well as recommendations to improve the observational sampling. Both issues are part of a long-term strategy to improve the knowledge about ocean dynamics and impacts in the Brazil current region.

**Acknowledgments** The authors would like to thank the logistical support provided by the Brazilian Navy Hydrographic Office (DHN) and the Brazilian GOOS Program. XBT probes were provided by NOAA/AOML, funded by the NOAA Office of Climate Observations. Mateus O. Lima, Mauro Cirano and Mauricio M. Mata were supported by Brazilian scholarships from the Brazilian Research Council-CNPq. This research was supported by PETROBRAS and approved by the Brazilian oil regulatory agency ANP (Agência Nacional de Petróleo, Gás Natural e Biocombustíveis), within the special participation research project Oceanographic Modeling and Observation Network (REMO). This work was also partially funded by CNPq and NSF. Partial support for Marlos Goes, Gustavo Goni, and Molly Baringer was provided by NOAA's Atlantic Oceanographic and Meteorological Laboratory and the Climate Observations Division of the NOAA Climate Program Office. The work presented using HYCOM/NCODA, GLORYS2V3, and FOAM has been carried out as part of the GODAE OceanView framework. HYCOM development has been supported over the course of several years by the Office of Naval Research, by the US Department of Energy, and by a grant from the National Ocean Partnership Program. GLORYS2V3 is supported by Mercator Ocean systems. FOAM is provided by the UK Met Office Ocean Forecasting R&D group. The altimeter products were produced by Ssalto/Duacs and distributed by Aviso, with support from Cnes (<http://www.aviso.altimetry.fr/duacs/>). We also thank the three anonymous reviewers for their thoughtful comments.

## References

- Biló TC, Silveira ICA, Belo WC, Castro BM, Piola AR (2014) Methods for estimating the velocities of the Brazil current in the pre-salt reservoir area off southeast Brazil. *Ocean Dyn* 64:1431–1446
- Bleck R (2002) An oceanic general circulation model framed in hybrid isopycnic-cartesian coordinates. *Ocean Model* 37:55–88

- Blockley EW, Martin MJ, McLaren AJ, Ryan AG, Waters J, Lea DJ, Mirouze I, Peterson KA, Sellar A, Storkey D (2014) Recent development of the Met Office operational ocean forecasting system: an overview and assessment of the new Global FOAM forecasts. *Geosci. Model Dev* 7:2613–2638. doi:10.5194/gmd-7-2613-2014
- Boebel O, Schmid C, Zenk W (1997) Flow and recirculation of antarctic intermediate water across the Rio Grande rise. *J Geophys Res* 102(C9):20967–20986
- Calado L, Gangopadhyay A, da Silveira ICA (2006) A parametric model for the Brazil current meanders and eddies off southeastern Brazil. *Geophys Res Lett* 33:L12602. doi:10.1029/2006GL026092
- Campos EJD (2006) Equatorward translation of the Vitoria Eddy in a numerical simulation. *Geophys Res Lett* 33:L22607. doi:10.1029/2006GL026997
- Campos EJD, Gonçalves JE, Ikeda Y (1995) Water mass structure and geostrophic circulation in the South Brazil bight – summer of 1991. *J Geophys Res* 100(C9):18537–18550
- Cheng L, Zhu J, Cowley R, Boyer T, Wijffels S (2014) Time, probe type, and temperature variable bias corrections to historical expendable bathythermograph observations. *J Atmos Oceanic Technol* 31:1793–1825. doi:10.1175/JTECH-D-13-00197.1
- Cummings JA (2005) Operational multivariate ocean data assimilation. *Q J R Meteorol Soc* 131:3583–3604
- Daley R (1991) Atmospheric data analysis. Cambridge University Press, Cambridge, p 457
- Davies T, Cullen MJP, Malcolm AJ, Mawson MH, Staniforth A, White AA, Wood N (2005) A new dynamical core for the met office's global and regional modelling of the atmosphere. *Q J Roy Meteorol Soc* 131:1759–1782. doi:10.1256/qj.04.101.6225–6230
- Dong S, Goni G, Bringas F (2015) Temporal variability of the meridional overturning circulation in the South Atlantic between 20S and 35S. *Geophys Res Lett* 42:7655–7662. doi:10.1002/2015GL065603
- Dotto TS, Kerr R, Mata MM, Azaneu M, Wainer I, Fahrbach E, Rohardt G (2014) Assessment of the structure and variability of Weddell Sea water masses in distinct ocean reanalysis products. *Ocean Science* 10:523–546. doi:10.5194/os-10-523-2014
- Drévillon M, Bourdallé-Badie R, Derval C et al (2008) The GODAE/Mercator-Océan global ocean forecasting system: results, applications and prospects. *J Oper Oceanogr* 1:51–57
- Evans DL, Signorini SR (1985) Vertical structure of the Brazil current. *Nature* 315(6014):48–50
- Goes M, Goni G, Keller K (2013) Reducing biases in XBT measurements by including discrete information from pressure switches. *J Atmos Ocean Tech* 30:810–824. doi:10.1175/JTECH-D-12-00126.1
- Goni GJ, Wainer I (2001) Investigation of the Brazil current front variability from altimeter data. *J Geophys Res* 106:31,117–31,128
- Goni GJ, Baringer MO (2002) Surface currents in the tropical Atlantic across high density XBT line AX08. *Geophys Res Lett* 9(24):2218. doi:10.1029/2002GL015873
- Goni GJ, Bringas F, Di Nezio PN (2011) Observed low frequency variability of the Brazil current front. *J Geophys Res* 116:C10037. doi:10.1029/2011JC007198
- Hunke EC, Lipscomb WH (2010) CICE: the Los Alamos sea ice model. Documentation and software users manual, Version 4.1 (LA-CC-06-012), T-3 Fluid Dynamics Group, Los Alamos National Laboratory, Los Alamos. 6221–6225
- Lentini C, Goni GJ, Olson D (2006) Investigation of Brazil current rings in the confluence region. *J Geophys Res* 111(C6):C06013. doi:10.1029/2005JC002988
- Madec G (2008) NEMO ocean engine, Note du Pole de modélisation, Institut Pierr Simon Laplace (IPSL), France, No 27 ISSN No. 1288–1619:6221–6223
- Mano MF, Paiva AM, Torres AR, Coutinho ALGA (2009) Energy flux to a cyclonic eddy off Cabo Frio, Brazil. *J Phys Oceanogr* 39:2999–3010. doi:10.1175/2009JPO4026.1
- Masina S, Storto A, Ferry N, Valdivieso M, Haines K, Balmaseda M, Zuo H, Drevillon M, Paren L (2015) An ensemble of eddy-permitting global ocean reanalyses from the MyOcean project. *Clim Dyn*. doi:10.1007/s00382-015-2728-5
- Mata MM, Cirano M, van Caspel MR, Fonteles CS, Goñi G, Baringer M (2012) Observations of Brazil current baroclinic transport near 22°S: variability from the AX97 XBT transect. *CLIVAR Exch* 58(17):5–10
- Mill GN, da Costa VS, Lima ND, Gabioux M, Guerra LAA, Paiva AM (2015) Northward migration of Cape São Tomé rings, Brazil. *Cont Shelf Res* 106:27–37
- Mogensen KS, Balmaseda MA, Weaver A (2012) The NEMOVAR ocean data assimilation system as implemented in the ECMWF ocean analysis for System 4, ECMWF. Tech Memo 668:6222–6226
- Müller TJ, Ikeda Y, Zangenber N, Nonato LV (1998) Direct measurements of the western boundary currents between 20°S and 28°S. *J Geophys Res* 103(C3):5429–5543
- Pereira J, Gabioux M, Marta-Almeida M, Cirano M, Paiva AM, Al A (2014) The bifurcation of the western boundary current system of the South Atlantic Ocean. *Revista Brasileira de Geofísica* 32(2):241–257
- Pham D, Verron J, Roubaud M (1998) A singular evolutive extended Kalman filter for data assimilation in oceanography. *J Mar Syst* 16:323–340
- Rocha CB, Silveira ICA, Castro BM, Lima JAM (2014) Vertical structure, energetics, and dynamics of the Brazil current system at 22°S–28°S. *J Geophys Res Oceans* 119:52–69. doi:10.1002/2013JC009143
- Schmid C, Schäfer H, Podesta G, Zenk W (1995) The Vitória Eddy and its relation to the Brazil current. *J Phys Oceanogr* 25:2532–2546
- Signorini SR (1978) On the circulation and the volume transport of the Brazil current between the Cape of São Tomé and Guanabara Bay. *Deep-Sea Res* 25:481–490
- Signorini SR, Miranda LB, Evans DL, Stevenson MR, Inostroza HMV (1989) Corrente do Brasil: estrutura térmica entre 19° e 25° S e circulação geostrófica. *Bolm Inst oceanogr* 37(1):33–49
- Silveira ICA, Schmidt ACK, Campos EJD, Godoi SS, Ikeda Y (2000) A Corrente do Brasil ao largo da costa leste brasileira. *Rev Bras Oceanogr* 48(2):171–183
- Silveira ICA, Calado L, Castro BM, Cirano M, Lima JAM, Mascarenhas AS (2004) On the baroclinic structure of the Brazil current-intermediate Western Boundary Current system. *Geophys Res Lett* 31(14):L14308. doi:10.1029/2004GL020036
- Silveira ICA, Lima JAM, Schmidt ACK, Ceccopieri W, Sartori A, Francisco CPF, Fontes RFC (2008) Is the meander growth in the Brazil current system off southeast Brazil due to baroclinic instability? *Dyn Atmos Oceans* 45:187–207. doi:10.1016/j.dynatmoce.2008.01.002
- Simmons A, Uppala S, Dee D, Kobayashi S (2006) ERA interim: new ECMWF reanalysis products from 1989 onwards. *ECMWF News* 110:25–35
- Soutelino RG, da Silveira ICA, Gangopadhyay A, Miranda JÁ (2011) Is the Brazil current eddy-dominated to the north of 20°S? *Geophys Res Lett* 38:L03607
- Stramma L, England M (1999) On the water masses and mean circulation of the South Atlantic Ocean. *J Geophys Res* 104(C9):863–883
- Thacker WC (2007a) Estimating salinity to complement observed temperature: 1. Gulf of Mexico. *J Mar Syst* 65(1–4):224–248. doi:10.1016/j.jmarsys.2005.06.008
- Thacker WC (2007b) Estimating salinity to complement observed temperature: 2. Northwestern Atlantic. *J Mar Syst* 65(1–4):249–267. doi:10.1016/j.jmarsys.2005.06.007
- Tsuchiya M (1985) Evidence of a double-cell subtropical gyre in the South Atlantic Ocean. *J Mar Res* 43:57–65

- Vianna ML, Menezes VV (2011) Double-celled subtropical gyre in the South Atlantic ocean: means, trends and interannual changes. *J Geophys Res* 116:C03024. doi:[10.1029/2010JC006574](https://doi.org/10.1029/2010JC006574)
- Vianna ML, Menezes VV, Chambers DP (2007) A high resolution satellite only GRACE based mean dynamic topography of the South Atlantic Ocean. *Geophys Res Lett* 34:L24604. doi:[10.1029/2007GL031912](https://doi.org/10.1029/2007GL031912)
- Wainer I, Gent, Goni G (2000) The annual cycle of the Brazil-Malvinas confluence region in the NCAR climate system model. *J Geophys Res* 105:26,167–26,177
- Zhao J, Johns W (2014) Wind-driven seasonal cycle of the Atlantic meridional overturning circulation. *J Phys Oceanogr* 44:1541–1562